Experiments on the Seasonal Variation of the General Circulation in a Statistical-Dynamical Model

YOSHIO KURIHARA

Geophysical Fluid Dynamics Laboratory, NOAA, Princeton University, Princeton, N. J. 08540

(Manuscript received 12 July 1972)

ABSTRACT

A study of the seasonal change of a climatic state of the atmosphere is made through the investigation of a response of a statistical-dynamical model to insolation having seasonal variation. Numerical experiments are performed for the two hypothetical cases: the land-covered earth (LCE) and the ocean-covered earth (OCE). The two cases differ in the thermal and aerodynamical conditions at the surface, and a hydrologic cycle is incorporated only in the model for OCE.

Numerical integrations are carried out until the same climatic state as one year before reappears. Then, annual marches of the zonal mean field, the eddy statistics, and the energetics are analyzed.

Baroclinicity at the middle latitudes is noticeable, in summertime, only for the OCE. Strong upper level easterly flow evolved at low latitudes for the LCE. The mean meridional circulation at low latitudes for both LCE and OCE is characterized by one big Hadley cell extending from the summer into the winter hemisphere. In the OCE, the water vapor is exported from the subtropics equatorward by the mean meridional circulation and poleward by large-scale eddies. The effect of ocean is to moderate the seasonal change of eddy activity so that the eddy transport of heat for the OCE is smaller in winter and larger in summer than that for the LCE.

The additional experiments show the dependency of the eddy statistics of the model on the internal viscosity. It is also shown that the after-effect of a sudden shock lasts about five months in the atmosphere for the OCE.

1. Introduction

The theme of this paper is the response of the atmosphere to an insolation having seasonal variation.

The atmosphere-ocean-land system receives the insolation which varies gradually with latitude and slowly with time except for a component of rather rapid diurnal change. Generally speaking, the effect of non-adiabatic heating which originates from solar radiation is to intensify the pre-existing baroclinicity of the atmosphere. This is counteracted by the heat transfer which tends to smooth out the meridional gradient of temperature. As a result of imbalance between the above two factors, the climate undergoes a seasonal variation. There may also be an oscillatory mode superposed on it.

It may be easily understood from the argument mentioned above that, in constructing a numerical model for investigating the aspects of seasonal variation of a climate, we should formulate the heating function in an appropriate way and also establish a reasonable scheme to estimate the transport of heat. Especially, the baroclinic wave has to be treated carefully, since it plays an important role in the heat budget.

Here, we will view some previous numerical models used in studying the variation of climate. For the two-layer, quasi-geostrophic model of Bryan (1959), non-adiabatic heating was of a Newtonian form. Its basic temperature field was determined from the forced temperature contrast and the forced static stability. The former was represented by one component of spherical harmonics and its amplitude varied sinusoidally with time. The forced lapse rate was related to the forced contrast of temperature between equator and pole. The specification of a truncated spectral method allowed a special type of Hadley circulation and a single disturbance of wavenumber 3 to occur. During the period of integration, the system remained fairly near the equilibrium. Kraus and Lorenz (1966) performed several experiments with a two-layer quasi-geostrophic model with Newtonian-type heating. The time variation of thermal equilibrium potential temperature was sinusoidal and the vertical stability was fixed to a prescribed value at each experiment. They assumed two different sets of heating function. One model could be compared to a sea-covered hemisphere; another had a schematic land-sea distribution along latitudes. A truncated spectral method retaining four waves was used for the integration, which showed the difference between the climates of spring and fall. The role of standing monsoon-type circulation was discussed too.

In the study of annual variation of atmospheric energy, Wiin-Nielsen (1970) adopted heating of Newto-

nian form. In his case, the equilibrium temperature was obtained from the formula of radiational balance as a function of latitude and time. The model was a two-layer, zonally averaged, quasi-geostrophic system. The eddy transfer of heat was estimated by making use of a diffusion coefficient.

Saltzman and Vernekar (1971) obtained an equilibrium state of the axially symmetric, vertically averaged component of climate for the given distribution of insolation. The zonally averaged form of a full set of thermo-hydrodynamical equations was used, and the barotropic and baroclinic wave theory was utilized to parameterize the eddy transport of heat and momentum. This kind of approach to the problem of long-term climatic change may be taken, if the change can be represented as a sequence of quasi-equilibrium states. However, even in such a case, it is probable that the seasonal variation has to be understood in order to obtain a climate at each phase of slow change.

The speculation stated above is based on the results obtained by Wetherald and Manabe (1972), wherein they noticed the effect of high-latitude warming when seasonal variation of insolation was included in their primitive equation model. This phenomenon was produced by the removal of snowpack in summer and by the change of state in the surface layer of the ocean. The model they used is a joint model of a nine-level ocean and a nine-level atmosphere. The non-adiabatic heating and the heat flux were explicitly computed at each grid point.

The numerical model we use in the present work is a two-layer statistical-dynamical model of the atmosphere (Kurihara, 1970). In the model, the heating of an air column is estimated from the insolation and the mean temperature of the air column in a parameterized way. This method was used for an experiment concerning seasonal variation of temperature in an atmosphere at rest, and its usefulness was shown (Kurihara, 1971). The meridional transport of heat due to large-scale eddies is computed by a prognostic formula derived from the baroclinic wave theory. The integrations are performed for the two hypothetical situations of a land-covered earth and an ocean-covered earth. Although we prescribe the observed annual mean values for albedo and static stability, we can still realize the problem areas of interest: e.g., 1) whether a persistent wind system will be established or not near the equator where it was windless in the experiment with the fixed annual mean insolation; 2) whether the baroclinicity of the atmosphere will be maintained or not in summer despite the fairly evenly distributed insolation; and 3) how the time variation of climate will be moderated by the presence of an ocean.

2. Numerical model

The detail structure of the statistical-dynamical model and mathematical notation are described in the author's previous paper (Kurihara, 1970) denoted as K.

In the model, the zonal mean wind and the eddy kinetic energy are predicted at the 250- and 750-mb surfaces, or levels 1 and 3, while the prognoses of zonal mean temperature and horizontal transport of heat by eddies are made at 500 mb or level 2. A diagnostic method is used for the estimate of eddy transport of momentum.

We assume two different kinds of system. In one case, the whole earth's surface is land; in the other the earth is covered entirely by ocean. Differences between the systems are incorporated into the numerical model through different specifications of the heating function and frictional force. This will be briefly described below. In particular, a hydrologic cycle is considered for the ocean-covered earth only.

a. The land-covered earth (LCE)

The land-covered earth and the associated atmosphere will be referred to as LCE.

The internal eddy viscosity is expressed by the formulas (5.1) and (5.3) of K. For the constants which appear in these formulas, we choose $\gamma=0.05$ and $l_v=30$ m. As a surface drag coefficient over land, we put $C_D=0.0043$.

Assuming that land has no heat capacity, we use a heat balance condition at the surface. The hydrologic cycle is not considered in the LCE system. Hence, the heating function at LCE can be estimated in the same way with that of the previous study. The only change we make is the insolation, whose latitudinal distribution is now no longer fixed but allowed to vary with time. The solar constant is assumed to be 2 ly min^{-1}.

The model atmosphere is assumed to be moistureless. However, it should be noted that the values of the parameters used for determining the heating function were derived from observed data. In this respect, the model is not completely free of the effect of moisture.

b. The ocean-covered earth (OCE)

The second system is called the ocean-covered earth and will be referred to as OCE. It has the same internal viscosity as that of LCE. The drag coefficient at the ocean surface is smaller than that for land. We put $C_D=0.0011$.

The thermodynamics of the OCE model is primarily determined by the prescribed temperature of the ocean surface and by the hydrologic cycle.

We specify the zonal mean of the sea surface temperature by

$$\bar{T}_*=T\text{SAV}\pm\frac{T\text{SRG}}{2}\sin\left(\frac{2\pi}{Y}t+\delta\right), \qquad (2.1)$$

where the positive and negative signs are used for the Northern and the Southern Hemisphere, respectively, TSAV is the annual mean of $\bar{T}_*$, TSRG is the range of

variation, Y represents a period of one year, t is time, and δ is a phase angle. We put $\delta=7\pi/6$ so that an extreme of $\bar{T}_*$ occurs at the end of February and August. Numerical values of TSAV and TSRG are shown in Fig. 1. The temperature obtained with those values for latitudes higher than 60° is approximately equal to the surface temperature observed in the arctic region; it is about the freezing point in summertime. For latitudes between 0° and 60°, the temperature computed with (2.1) agrees well with the zonal average of the observed sea surface temperature. It is always above the freezing point. Fig. 2 shows $\bar{T}_*$ at the March equinox and the June solstice as a function of latitude. A large variation at high latitudes both with time and with space is seen.

The prescribed surface temperature is used for the estimate of the longwave radiation emitted from the surface, i.e., $s\bar{T}_*^4$ where s is the Stephen-Boltzmann constant. Except for this term, the scheme to estimate the heating of an air column due to radiation is quite similar to that in K.

For the OCE, we need the zonal mean temperature at the 1000- and 850-mb levels. These are obtained from the temperature at level 2 and the static stability Γ_2 by using the empirically determined formulas

$$\bar{T}_{1000}=1.133\bar{T}_2+96.71\Gamma_2, \tag{2.2}$$

$$\bar{T}_{850}=1.082\bar{T}_2-40.8\Gamma_2, \tag{2.3}$$

where temperature is in °K and Γ_2 in °K mb^{-1}. The derivation of the empirical formulas (2.2)–(2.7) is discussed in the Appendix.

Using $\bar{T}_*$ and $\bar{T}_{1000}$, we can estimate the warming rate of an air column due to sensible heat flux (SHFX)

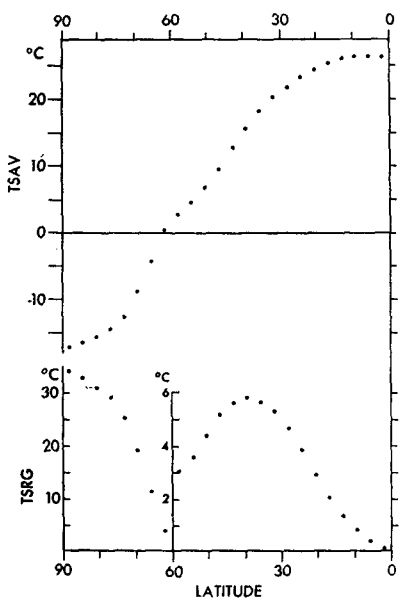

FIG. 1. Latitudinal distribution of TSAV and TSRG in Eq. (2.1).

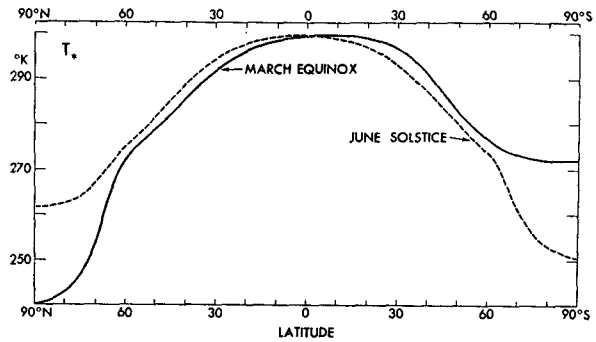

FIG. 2. Latitudinal distribution of the zonal mean sea surface temperature at the March equinox and the June solstice.

across the ocean surface. An empirical formula is

$$\mathrm{SHFX}=\frac{g}{c_p\bar{p}_*}0.0105(\bar{T}_*-\bar{T}_{1000}), \tag{2.4}$$

where SHFX is in °K day^{-1}, if g, c_p, $\bar{p}_*$ and temperature are expressed in cm sec^{-2}, cal gm^{-1}(°K)$^{-1}$, mb and °K, respectively.

The effect of the hydrologic cycle on the heating function is to give an additional component through the release of latent heat by condensation of water vapor. If the evaporation at the ocean surface, the condensation, and the flux of moisture can be reasonably estimated, then it may be possible to predict the moisture content of the air with little error. However, this is difficult when a numerical model with low vertical resolution is used. Instead, we decided to estimate the amount of moisture diagnostically, use it for the calculation of evaporation and the flux of moisture, and then determine the precipitation from a balance condition of water vapor. It will be shown later that such a scheme is adequate.

The diagnostic formulas which give the mixing ratio r of water vapor at the 1000- and 850-mb levels are

$$\bar{r}_{1000}=\bar{s}_{1000}\left(0.6915+0.08119\frac{P}{E}\right), \tag{2.5}$$

$$\bar{r}_{850}=\bar{s}_{850}\left(0.6227+0.1408\frac{P}{E}\right). \tag{2.6}$$

In (2.5) and (2.6), $\bar{s}_{1000}$ and $\bar{s}_{850}$ are the saturation mixing ratio at $\bar{T}_{1000}$ and $\bar{T}_{850}$, respectively, P is the precipitation rate, and E evaporation. In the numerical integration, we use the values of P and E at the previous time level.

An empirical formula for computing the rate of evaporation at the sea surface is

$$E=0.0211(\bar{s}_*-\bar{s}_{1000})+0.02272(\bar{s}_*-0.45\bar{r}_{1000}), \tag{2.7}$$

where E is in gm cm^{-2} day^{-1} when the mixing ratio is given in gm kg^{-1}.

We can make an approximate estimate of the vertically integrated meridional transport of moisture from

$$\int_0^1 \overline{rv}\,\bar{p}_*\frac{d\sigma}{g}=\frac{\bar{p}_*}{g}\left[0.75\bar{r}_{850}\bar{v}_3+0.3\left(\frac{d\bar{s}}{dT}\right)_{850}\overline{\bar{r}_{850}T'v'_2}\right], \quad (2.8)$$

where arbitrary numerical constants are chosen appropriately. The two factors on the right-hand side represent transports by the mean meridional circulation and by the eddies, respectively.

As mentioned above, we assume a balance condition for water vapor. Thus, the sum of the rate of evaporation and the convergence of moisture gives the precipitation intensity P:

$$P=E-\frac{\partial}{\alpha\cos\theta\partial\theta}\int_0^1 \overline{rv}\,\bar{p}_*\cos\theta\frac{d\sigma}{g}. \quad (2.9)$$

Multiplying P by the latent heat constant and dividing the product by the heat capacity of the air column, we finally get the heating rate of air column due to the condensation of water vapor, i.e.,

$$\mathrm{COND}=\frac{PL}{c_p\bar{p}_*/g}. \quad (2.10)$$

3. Numerical integrations

The grid system of the present model and the finite difference scheme are the same with those used in K; namely, there exists 48 zonal rings with the same latitudinal width between the two poles.

The numerical integration for LCE was made as follows: At first, the state at 150 days for the fixed annual mean insolation was obtained as in K except that the friction coefficients specified for LCE were used. At this stage the time was taken to be equivalent to the 100th day of the first year and the insolation started to vary with time. The numerical integration was continued up to day 50 of the third year. A comparison between the two states one year apart indicated that the iteration in the third year was almost a repeat of the one in the second year. Accordingly, the analysis was made for the data of the second year.

In case of OCE, the first phase of the integration was the same as that for LCE. After 100 days, the drag coefficient was decreased gradually to the value for OCE. The state at 150 days thus obtained was set to the initial state of the annual iteration experiment for OCE. Time was set to the 100th day of the first year. The insolation started to vary with season and the effect of the hydrologic cycle was introduced at that time. The results of integration early in the fifth year were almost similar to those at the corresponding period in the fourth year. Therefore, the data for the fourth year were considered as typical for the annual iteration for OCE.

In the following sections, the annual iterations of the various quantities of the LCE and OCE systems are presented in the figures. Unless otherwise mentioned, they were prepared from data taken every 8 days.

In the analyses of the results, we place stress on the differences between the climates of the LCE and OCE systems. It should be noted here that the seasonal variation of the actual atmospheric state has been analyzed in recently published fine work by Oort and Rasmusson (1971).

4. Variation of zonal mean temperature field with time

Seasonal variations of the zonal mean temperature at level 2, which is near 500 mb, are shown in Fig. 3, separately for LCE and for OCE.

The difference in baroclinicity for the two cases is clearly seen. At LCE, the heating at the middle latitudes in the summer hemisphere and the cooling at the winter polar night region are very large, since the land is assumed to have no heat capacity. Consequently, the annual range of temperature is large at every latitude. The maximum temperature is observed at 40S in January and shifts to 40N in July. The intensity of baroclinicity at middle latitudes is almost zero in summer.

In case of OCE, the temperature field is affected by an enormous heat capacity of the ocean and also by a hydrologic cycle. The range of temperature variation is smaller than that for LCE. The latitude of maximum temperature is found to be in the summer hemisphere near the equator. Comparing the meridional gradient of temperature with that for LCE, we see that the effect of the ocean is to moderate the seasonal change of baroclinicity by weakening it in winter and significantly intensifying it in summer.

The time lag of extreme temperatures behind the solstices at the middle latitudes is about one month for the LCE. This is almost the same as occurs in the experiment for an atmosphere at rest (Kurihara, 1971). The lag is due to the heat capacity of the atmosphere. For the OCE, the time lag is about $1\frac{1}{2}$ months. Note that the specified sea surface temperature has extreme lag values of about 2 months behind the solstices.

It is interesting to note that the global mean temperature for the LCE is higher in January than in July. This is apparently caused by the seasonal difference in the distance of the earth to the sun.

Some analyses concerning the annual iteration of the zonal mean temperature are made in the following subsections.

a. Heating rate

Latitudinal distributions of the net rate of nonadiabatic heating of an air column at the March equinox and June solstice are presented in Fig. 4 for LCE and for

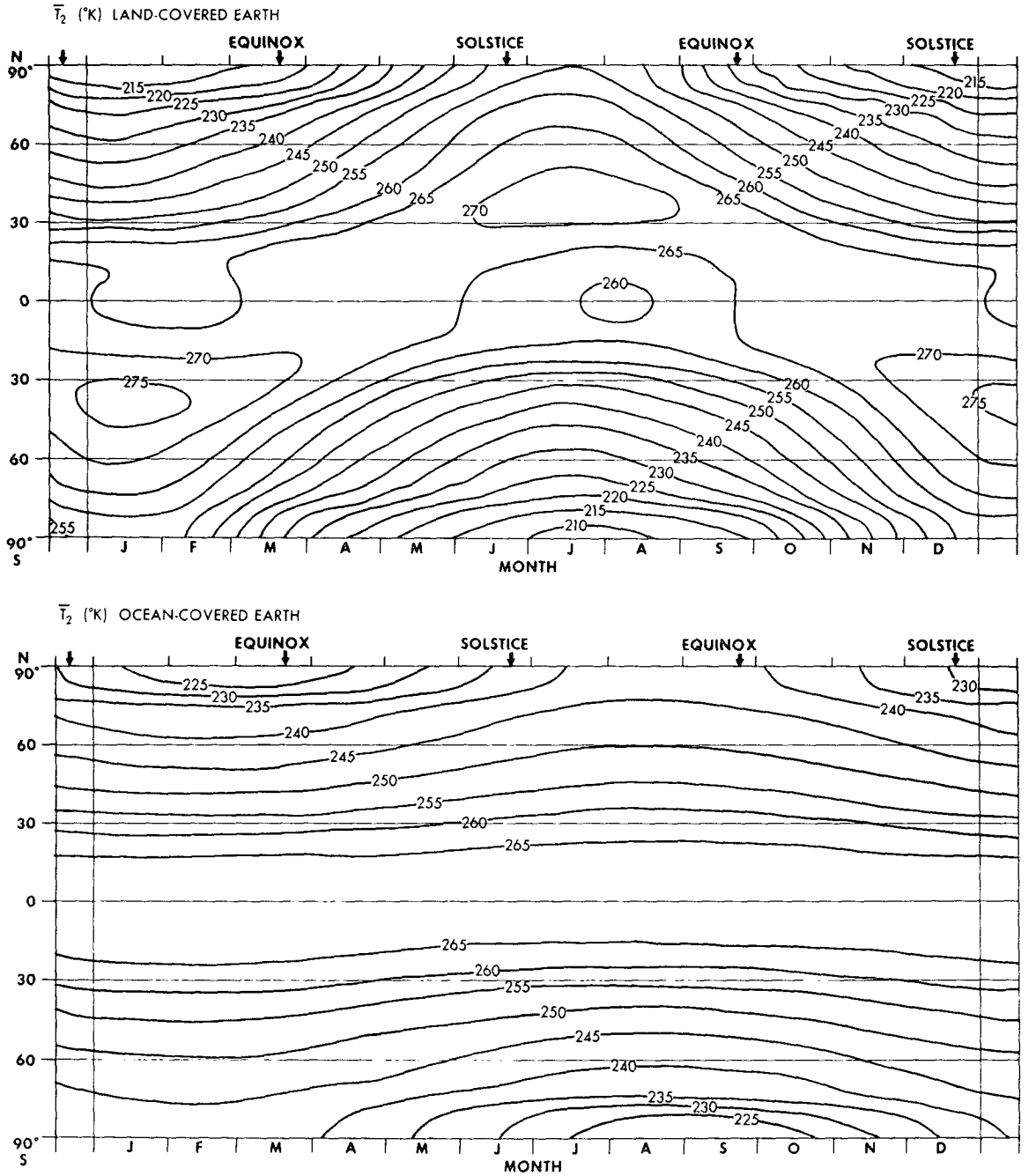

FIG. 3. Time variation of the latitudinal distribution of zonal mean temperature at level 2, for LCE and OCE.

OCE, respectively. The components of the heating function are also shown.

For LCE, the heat balance condition at the surface requires that a large amount of sensible heat be transported upward across the surface. Exceptions are seen at high latitudes during the equinox and also in the winter polar night region.

The net heating rate for the OCE is quite different from that for the LCE. It has three maxima both at the equinox and at the solstice. It is difficult to single out a component of heating function to which the above-mentioned distribution of the net heating rate can be primarily ascribed. However, it is apparently caused, directly or indirectly, by the hydrologic cycle and the presence of the ocean.

At the solstice, the net effect of heating components is to cool the atmosphere in most of the winter hemisphere in case of LCE. For the OCE, the area of strong net

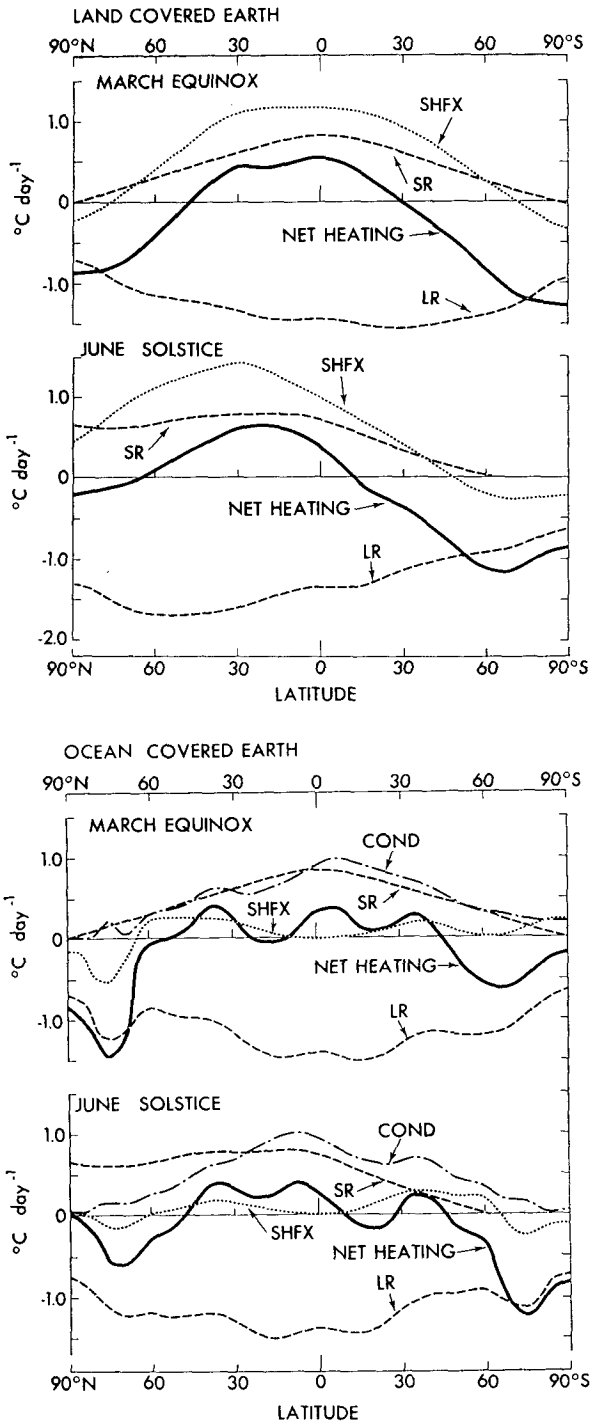

FIG. 4. Latitudinal distribution of the mean heating rate for the total air column due to shortwave radiation (SR), longwave radiation (LR), heat flux at the earth's surface (SHFX), condensation of water vapor (COND), and the net effect (NET HEATING).

cooling is seen at high latitudes only. The latitudinal variation of heating rate in the summer hemisphere for the OCE is about double that of the LCE. This may be a contributing factor in the maintenance of the baroclinicity in the summertime for the OCE.

b. Effect of dynamics on temperature change

The time change of temperature is obtained when the dynamical effect is added to the rate of diabatic heating discussed in the preceding subsection. The dynamical effect is divided into three components: the effect due to mean meridional motion, that due to eddy motion, and that due to sub-grid scale horizontal diffusion. Those three effects together with the diabatic heating and the resulting tendency at the March equinox and the June solstice are shown in Fig. 5 for LCE and OCE, respectively. The effect of horizontal diffusion is always small everywhere.

At the equinox, for both the LCE and OCE systems, the warming due to diabatic process in tropical latitudes is counterbalanced by the effect due to the meridional circulation. In middle latitudes, the cooling due to eddy transport of heat more or less balances the effect due to both meridional circulation and diabatic heating. At higher latitudes, the diabatic cooling is largely balanced by the eddy transport.

At the solstice, the winter hemisphere resembles to some degree its state at the equinox. In the summer hemisphere, however, a large amount of heating is mostly balanced by the mean meridional circulation for the LCE. On the other hand, for the OCE, the eddy transport is most important, being a reflection of the summertime activity of baroclinic waves for the OCE.

Generally speaking, the temperature changes by the different mechanisms are so well balanced that the net rate of change of zonal mean temperature varies smoothly with latitude. This rate is particularly small for the OCE.

c. Zonal available potential energy

Estimates of the zonal available potential energy for the entire global domain and the contribution to it from the Northern Hemisphere are given in Table 1. The monthly mean values therein are the averages of daily statistics.

For the LCE, the seasonal change of zonal available potential energy is very large. The global integral shows that the variation is semiannual wlth a range of 744 J cm^{-2}. The hemispheric contribution to the global integral becomes large in winter because of the strong baroclinicity.

On the other hand, the seasonal variation of zonal available potential energy for the OCE is small. Its annual range is only 72 J cm^{-2}. This annual average is about 62% of that of the LCE.

d. Ocean heat storage

In the OCE experiment, one can estimate the heat that enters the ocean from the heat budget at the ocean surface. The result is shown in Fig. 6.

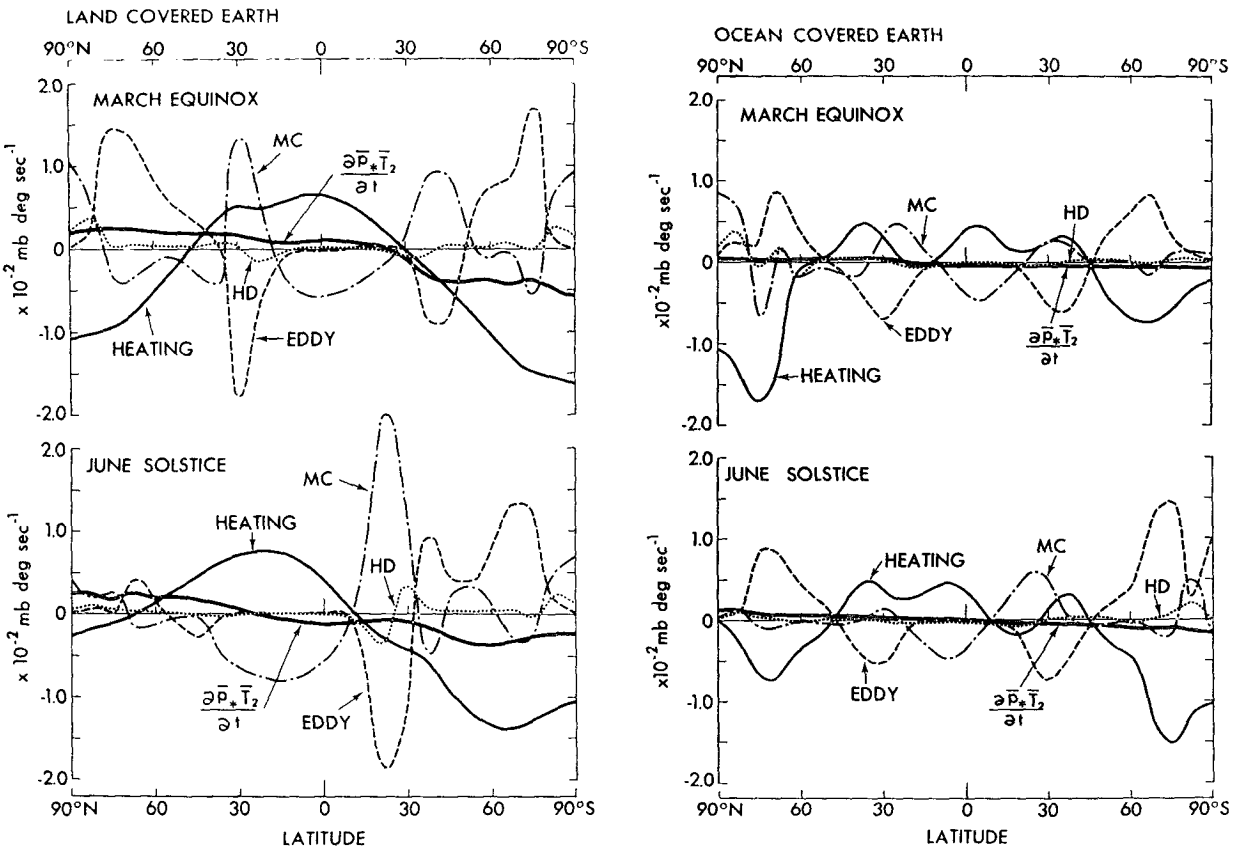

FIG. 5. Latitudinal distribution of change of $\bar{p}_*\bar{T}_2$ due to non-adiabatic heating (HEATING), meridional circulation (MC), large-scale eddies (EDDY), horizontal diffusion (HD), and the net effect ($\partial\bar{p}_*\bar{T}_2/\partial t$).

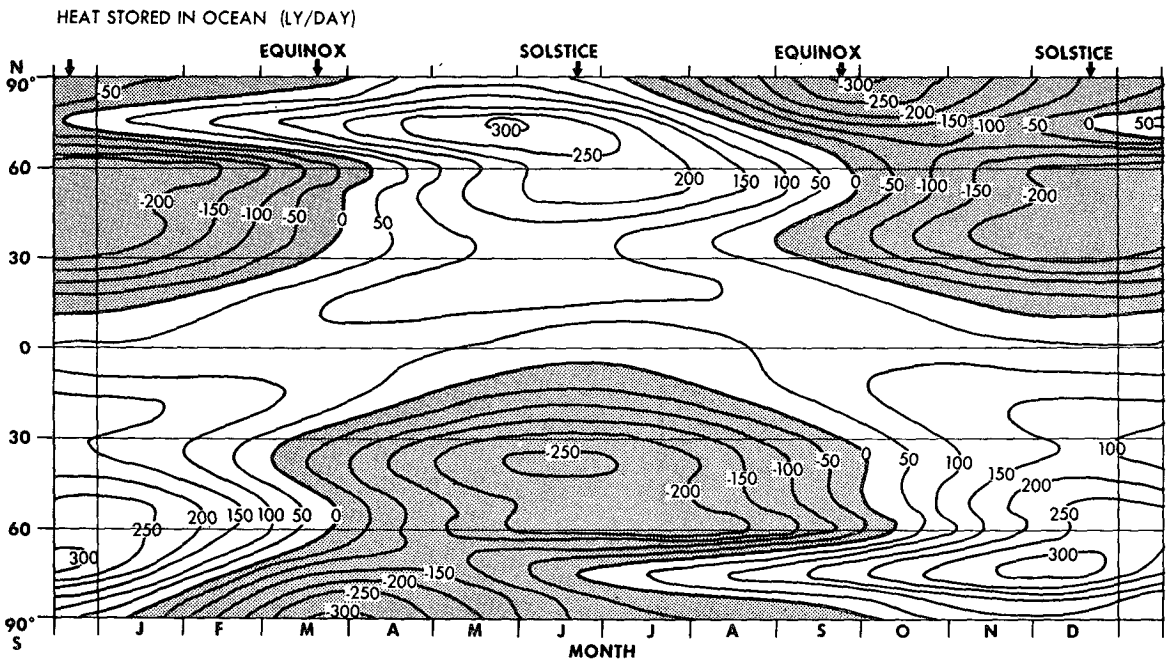

FIG. 6. Time variation of the latitudinal distribution of heat which entered the ocean.

TABLE 1. Zonal available potential energy (P_Z; J cm^{-2}) for the entire global domain and the contribution to it from the Northern Hemisphere. The monthly values are the averages of daily statistics.

	Month												Annual
	Jan.	Feb.	Mar.	Apr.	May	June	July	Aug.	Sep.	Oct.	Nov.	Dec.	
Land-covered earth													
Global mean	1355.0	1034.0	746.3	611.0	718.1	1086.0	1302.0	1034.0	758.8	623.8	718.0	1121.0	925.7
Northern Hemisphere	1925.0	1475.0	1041.0	593.8	385.8	563.5	754.7	599.0	447.1	610.7	1039.0	1663.0	924.8
Ocean-covered earth													
Global mean	578.1	609.2	604.8	570.1	538.1	537.4	572.1	606.3	605.7	572.4	539.8	540.2	572.8
Northern Hemisphere	759.7	825.9	797.0	687.7	556.3	451.4	398.5	390.8	410.8	452.6	523.9	633.0	574.0

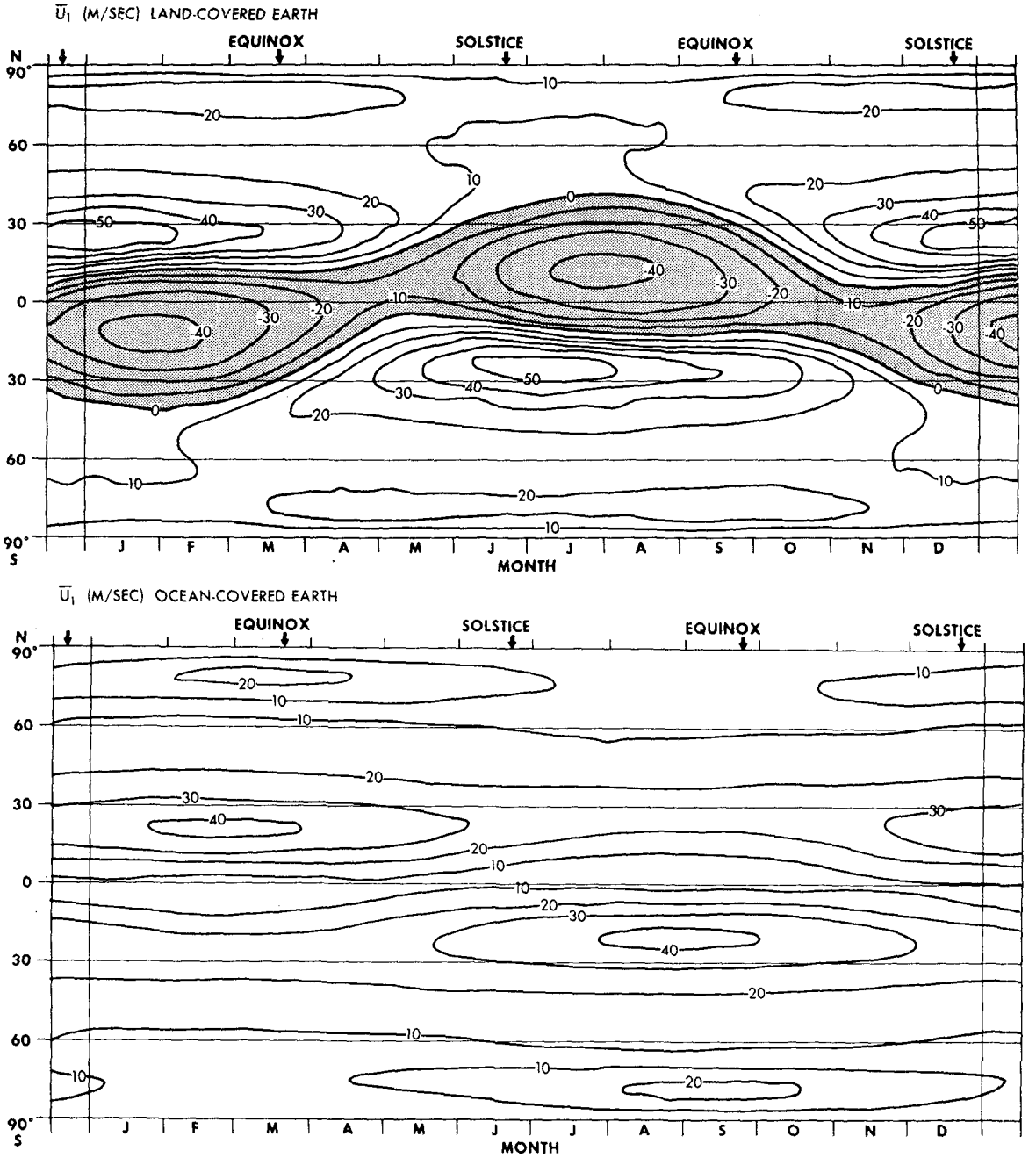

FIG. 7. Time variation of the latitudinal distribution of zonal mean of zonal wind at level 1, for LCE and OCE.

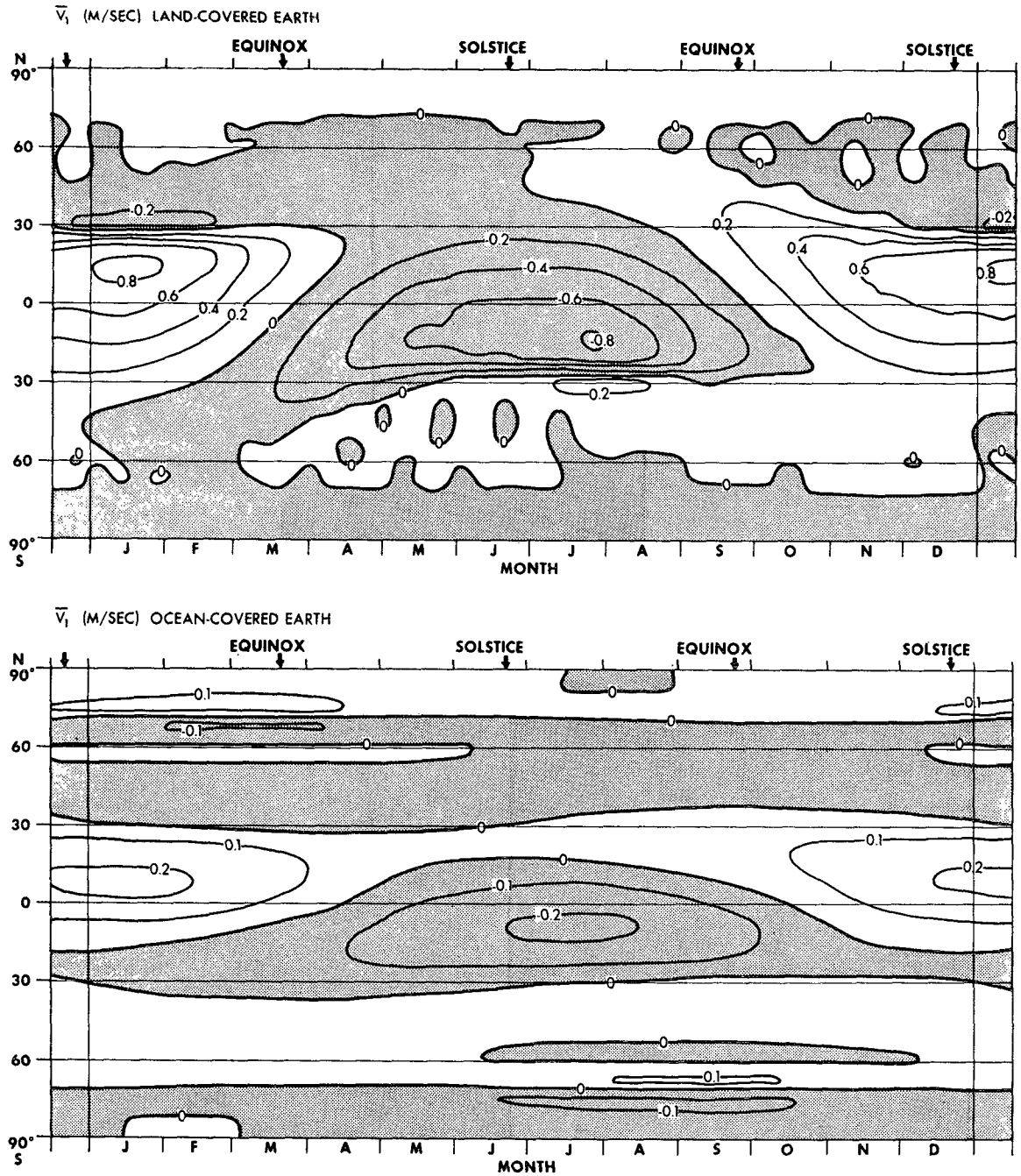

FIG. 8. Time variation of the latitudinal distribution of mean meridional flow at level 1, for LCE and OCE.

During the summertime, a large amount of heat enters the ocean. The ocean loses heat during the wintertime. In Fig. 6, the amount of 100 ly day^{-1} is equivalent to the atmospheric warming of 0.5 in the units used in Fig. 5, i.e. in 10^{-2} K mb sec^{-1}. Comparing its value with the rate of heating of atmosphere due to diabatic processes, we see that the heat stored in the ocean is not negligible at all.

The heat stored in the ocean is not necessarily related to the local change of ocean temperature, as the heat can be transported vertically and horizontally.

5. Variation of zonal mean wind field with time

In this section, we discuss the field of zonal mean wind which clearly shows the effect of seasonal variation of insolation. When an atmosphere receives a fixed annual mean insolation, calm prevails at the tropical latitudes and it is windless at the equator (Fig. 8 in K).

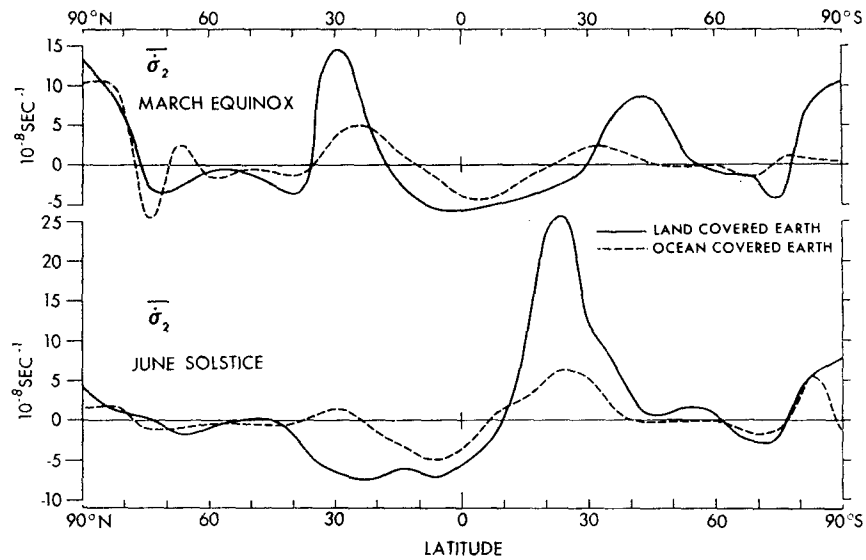

FIG. 9. Latitudinal distribution of the mean vertical motion at level 2 at the March equinox and the June solstice.

In contrast to this, when the seasonal variation of insolation is included in a model, a fairly persistent system of zonal wind is established at the tropical latitudes as will be shown in the following. Furthermore, a cross-equatorial meridional flow which has a semi-annual cycle appears. It should be noticed too that the difference between the LCE and OCE systems shows up dramatically in the zonal mean wind field.

a. Zonal component of wind

The latitude and time variations of the zonal mean of the zonal component of wind at level 1, i.e. at

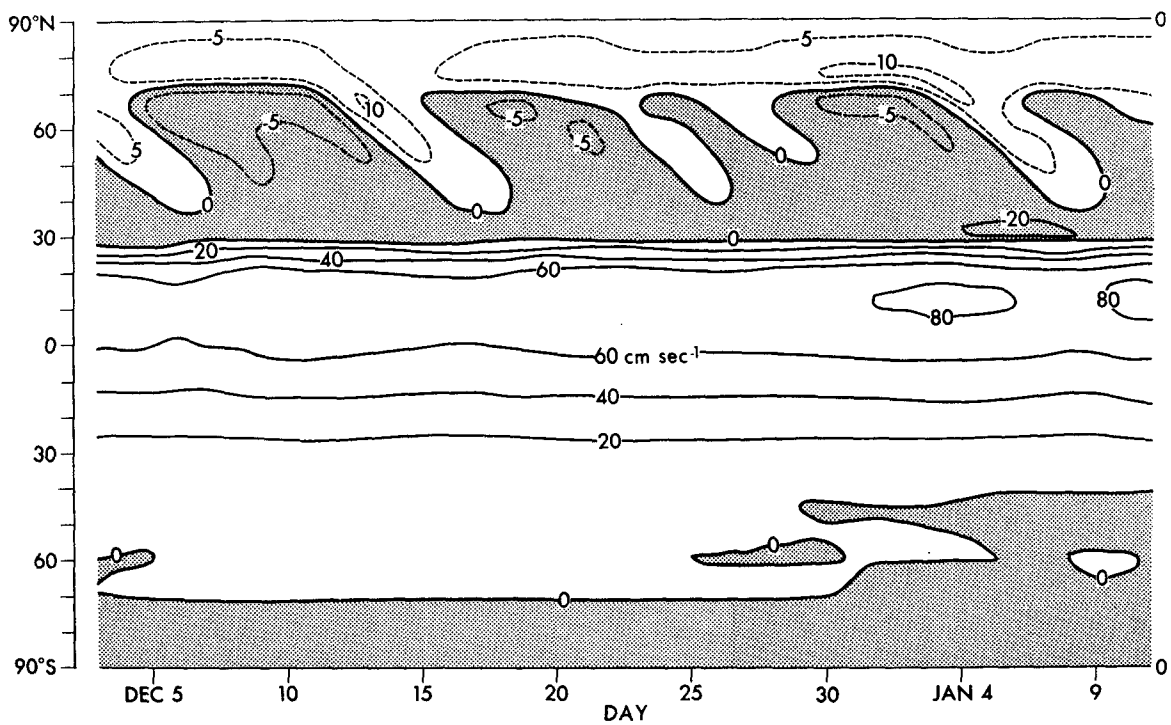

FIG. 10. Time variation of the latitudinal distribution of mean meridional flow at level 1 for LCE for the period 4 December through 10 January. Contours are drawn based on daily values.

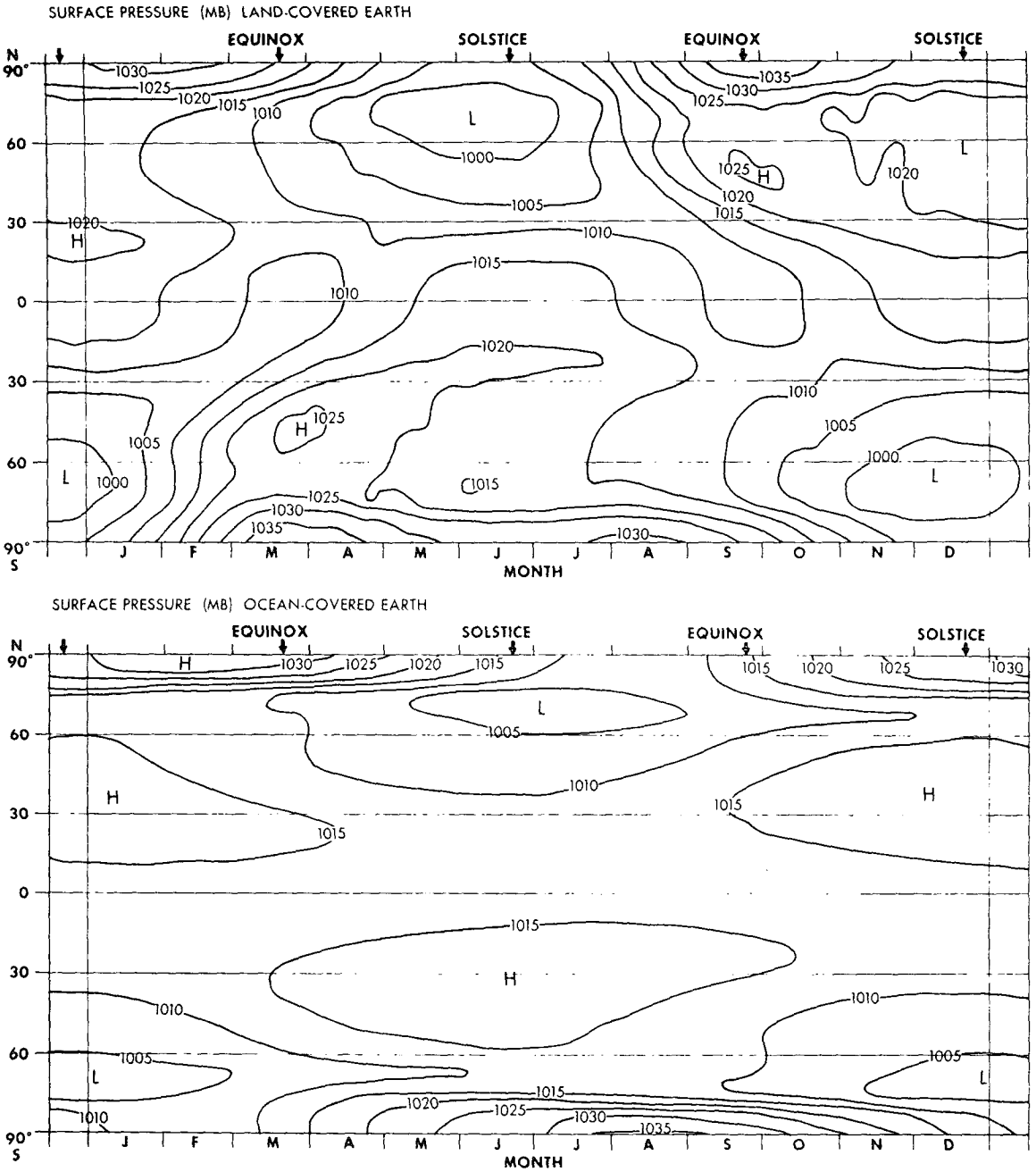

FIG. 11. Time variation of the latitudinal distribution of zonal mean surface pressure, for LCE and OCE.

the 250-mb level, for LCE and OCE are shown in Fig. 7.

Only in the LCE are strong easterly winds found at level 1. This easterly flow in low latitudes has a maximum intensity in the summer hemisphere. In spring and fall, the easterly flow is relatively weak. The semi-annual component is predominant in the variation of zonal flow at a narrow belt near the equator. In the subtropics, a strong westerly flow is observed during the winter. A double jet structure occurs in the winter hemisphere. The zonal flow is symmetric with respect to the equator only in late April and late October.

The results from the integration for LCE indicate that the position of the maximum of the easterly flow occurs in the summer hemisphere at level 1, but is located in the winter hemisphere at lower levels. Although the figures for lower levels are not shown, the maximum at level 3 is located near the equator. At level 4, i.e., at the surface, the easterly is strongest in the winter hemisphere. Very weak westerly flow occurs at

TABLE 2. Kinetic energy of zonal mean flow (K_Z; J cm^{-2}). Mean values for the global domain and for the Northern Hemisphere are shown.

	Month												Annual
	Jan.	Feb.	Mar.	Apr.	May	June	July	Aug.	Sep.	Oct.	Nov.	Dec.	
Land-covered earth													
Global mean	247.4	212.3	149.6	97.4	106.0	174.9	237.7	211.3	153.5	101.3	105.7	178.4	164.6
Northern Hemisphere	304.0	232.6	175.4	106.8	51.3	90.5	183.4	192.3	128.3	87.7	157.4	266.3	164.7
Ocean-covered earth													
Global mean	126.0	130.4	129.6	123.7	119.3	120.4	125.5	130.1	129.9	124.3	119.9	121.2	125.0
Northern Hemisphere	174.6	193.0	190.8	167.6	133.9	101.8	79.3	68.0	67.9	79.6	105.6	141.6	125.3

the surface near the equator in late June and late December.

As seen in Fig. 7, the zonal wind at level 1 for the OCE is always westerly. Its minimum which is about 5 m sec^{-1} is found near the equator. The weak westerly flow at the equator is apparently due to the convergence of relative angular momentum by eddy flux and diffusion. In the Northern Hemisphere a westerly flow in the subtropics attains its maximum intensity in February. This maximum occurs later than that of the LCE by more than one month.

At the surface in the OCE, the zonal flow in low latitudes is weak easterly the whole year. Its maximum is found in the winter hemisphere.

b. Meridional circulation

The variation of the meridional component of wind with latitude and time at level 1 in LCE and OCE is shown in Fig. 8. The latitudinal distribution of vertical motion at level 2 at the March equinox and the June solstice is seen in Fig. 9, where positive values denote downward motion.

In the LCE a big Hadley circulation is a predominant feature most of the time. It has a broad region of upward motion in the summer hemisphere (Fig. 9), cross-equatorial flow toward a winter hemisphere at level 1 (Fig. 8), and a fairly strong downward current in the subtropics in the winter hemisphere (Fig. 9). The meridional flow reaches its maximum value, 80 cm sec^{-1}, in January and in July. Two Hadley circulations which are symmetrical about the equator occur for short periods around the equinox. A Ferrel cell exists in the winter hemisphere only. Its short-period oscillation will be discussed later. A direct circulation always occurs in high latitudes.

The meridional circulation in the OCE is characterized by the three-cell structure in both hemispheres. There exist two Hadley circulations in low-latitude regions. Except for short periods about half a month after the solstices, one of the cells extending from the summer into the winter hemisphere is more intense than

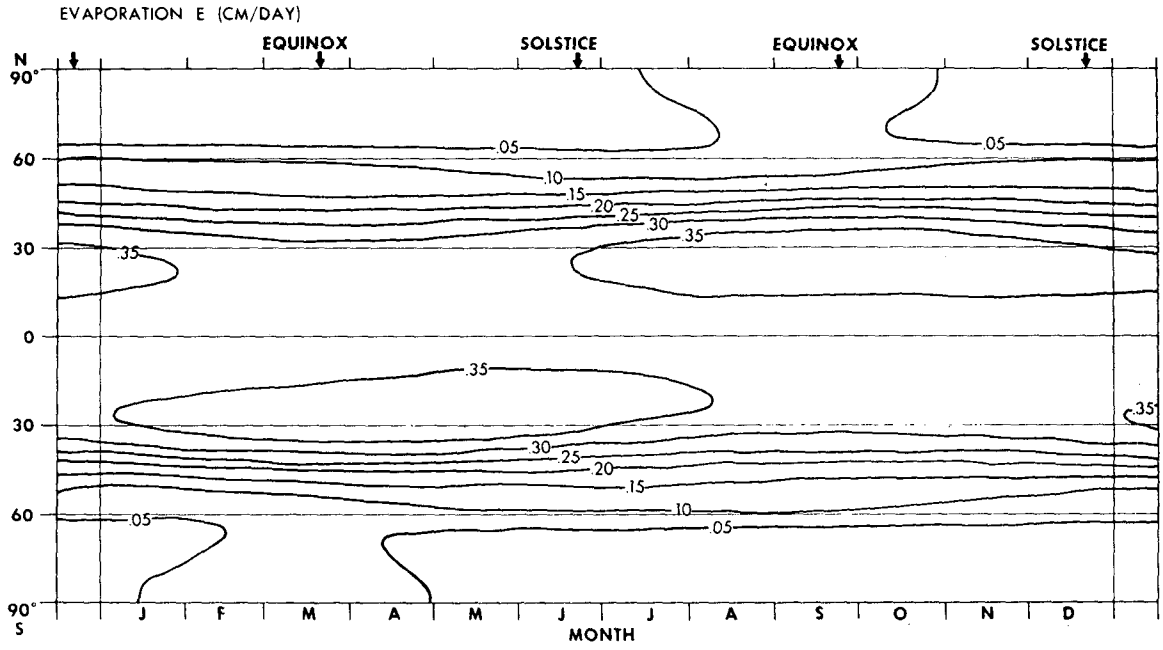

FIG. 12. Time variation of the latitudinal distribution of evaporation (E), precipitation (P), and $E-P$, for OCE.

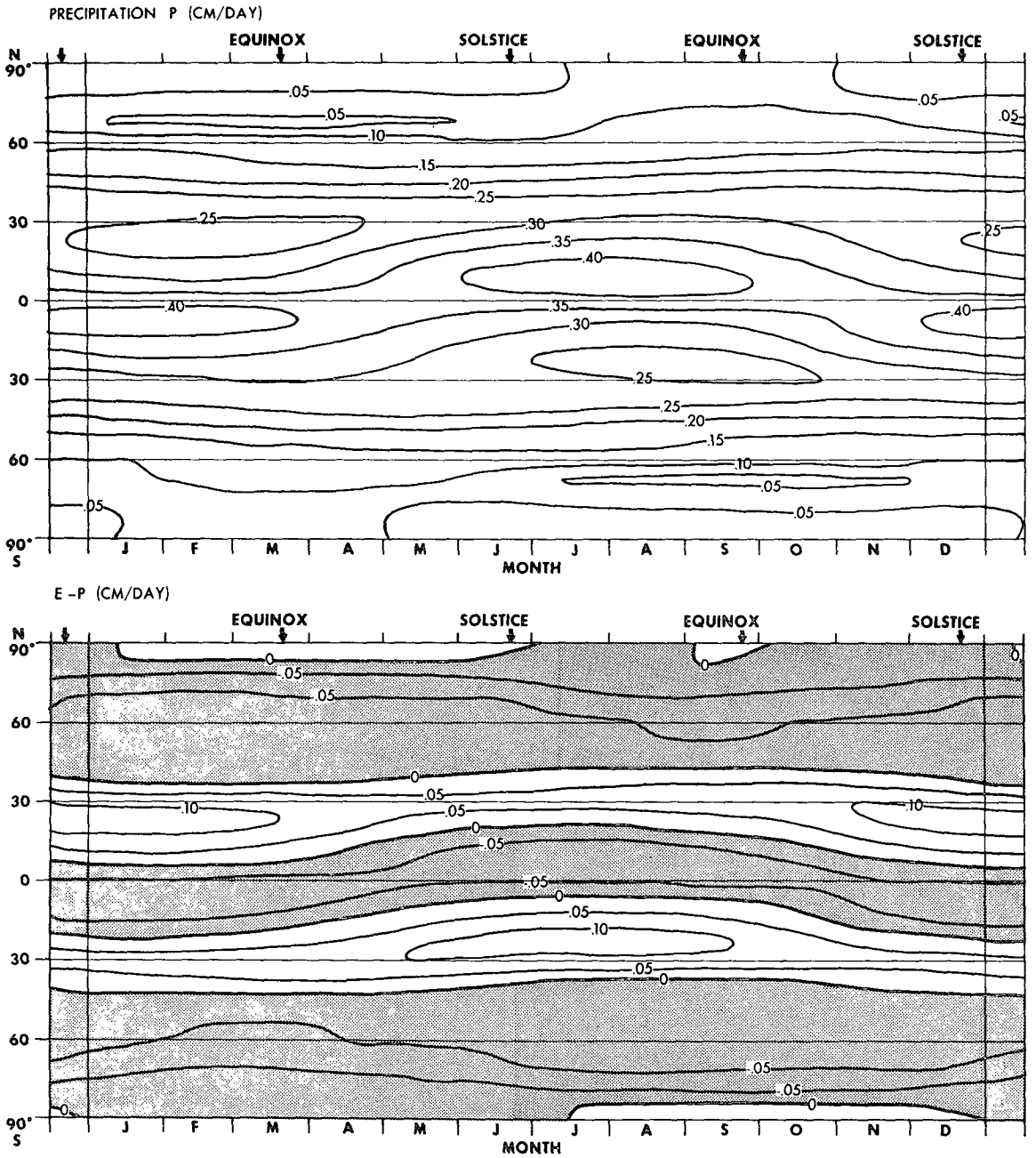

FIG. 12. (*continued*).

the other. The maximum meridional speed is, however, about one-fourth of that occuring in the LCE. As for the Ferrel cell, its time variation is weak in comparison with that of the LCE.

c. Fluctuation of the Ferrel cell of the LCE *with time*

In the experiment with an annual mean insolation, it was shown that Ferrel cells were apparently formed one after another at a high latitude and then propagated southward (Fig. 6 in K). In the present study, a similar fluctuation of the Ferrel cell is obtained in the LCE system. Fig. 10 shows the time variation of the meridional flow at level 1 for the period 4 December through 10 January, based on daily values. Successive evolution of the Ferrel cell in the winter hemisphere is seen. On certain occasions, e.g. 16 December, we obtain a five-cell structure in the Northern Hemisphere.

d. Kinetic energy of the zonal mean flow

The averages of the daily values of kinetic energy of zonal mean flow are estimated for each month for the

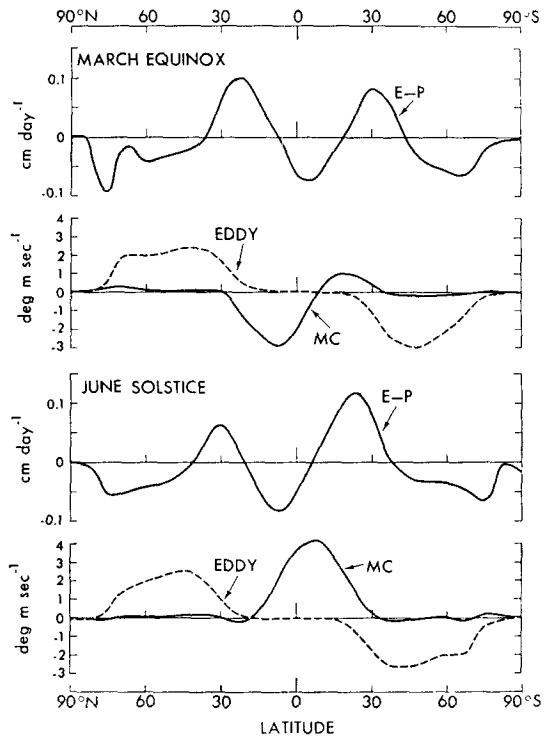

FIG. 13. Latitudinal distribution of evaporation minus precipitation ($E-P$), meridional flux of moisture due to mean meridional circulation (MC), and that due to large-scale eddies (EDDY), at the March equinox and the June solstice. MC and EDDY are expressed in latent heat flux divided by specific heat at constant pressure.

entire global domain and also for the Northern Hemisphere. These statistics are presented in Table 2.

In the Northern Hemisphere of the LCE, a primary peak of the kinetic energy of zonal mean flow appears in the wintertime and a secondary peak in the summertime. The former peak is due to the strong westerly flow and the latter to the strong easterly wind. The lowest value, reached in May, is about one-sixth of the highest value. Another minimum occurs in October. Since the Southern Hemisphere produces similar features with the phase difference of half a year, a semi-annual variation is a predominant component in the global integral.

The semi-annual variation of the global mean kinetic energy is also seen in OCE. However, its amplitude is only 4.5% of the annual mean value. In the hemispheric statistics, one maximum and one minimum are obtained in March and September, respectively. It differs from LCE in that the energy of zonal mean flow does not increase in summertime. This is because a strong easterly flow does not exist in the summertime in OCE.

6. Variation of zonal mean surface pressure with time

In the present model, the surface pressure does not vary along latitude circles; it is a function of latitude and time. The computed results for LCE and OCE are presented in Fig. 11.

For the LCE, the variation of zonal mean surface pressure is large in comparison with the actual variation. The pressure in middle latitudes in summer is very low and that in low latitudes is unrealistically high. Such a large shift of air mass from the middle latitudes of the summer hemisphere toward the equatorial area and further into the winter hemisphere is apparently related to the Hadley circulation.

The variation of surface pressure in OCE is small. In the subtropics a very weak high pressure belt is formed in summer, although it is not seen in the figure because of the contour interval used.

In the actual atmosphere, we observe a contrast of pressure system and its seasonal change between the land and the ocean areas. Lack of similarity between the present results for LCE and OCE and the actual distribution of pressure over land and ocean, respectively, suggests that a longitudinal shift of air mass is probably important in determining the field of air mass in the actual atmosphere.

7. Hydrologic cycle in OCE

We mentioned in Section 2 that evaporation in the OCE system was estimated by an empirical formula and that precipitation was computed from a diagnostic scheme. The results thus obtained during the course of integration are shown in Fig. 12.

Maximum evaporation occurs in the subtropics of both hemispheres. It amounts to more than 10 cm month^{-1} but is slightly diminished in the springtime. A weak minimum in evaporation is always seen near the equator. This is probably due to the relatively wet condition in this region associated with convergence of moisture.

Precipitation, on the other hand, has a maximum in the tropical latitudes of the summer hemisphere; it exceeds 12 cm month^{-1}. The area of large rainfall shifts from one hemisphere to another in late April and in late October. This shift is apparently related to the time variation of the Hadley cells which play an important role in the moisture budget. In the winter hemisphere, precipitation is minimum in the subtropics and it increases slightly poleward of it.

The difference between evaporation and precipitation is also shown in Fig. 12. In the subtropics, evaporation always exceeds precipitation, especially in winter. At all other latitudes, the precipitation exceeds the local evaporation. Since the moisture content of the air at each latitude varies little with time, these excesses imply an export of moisture from the subtropics to both lower and higher latitudes.

Analysis of the transport of latent heat is made at the time of the March equinox and the June solstice. In Fig. 13, the flux of moisture, expressed as latent heat flux divided by specific heat at constant pressure, pro-

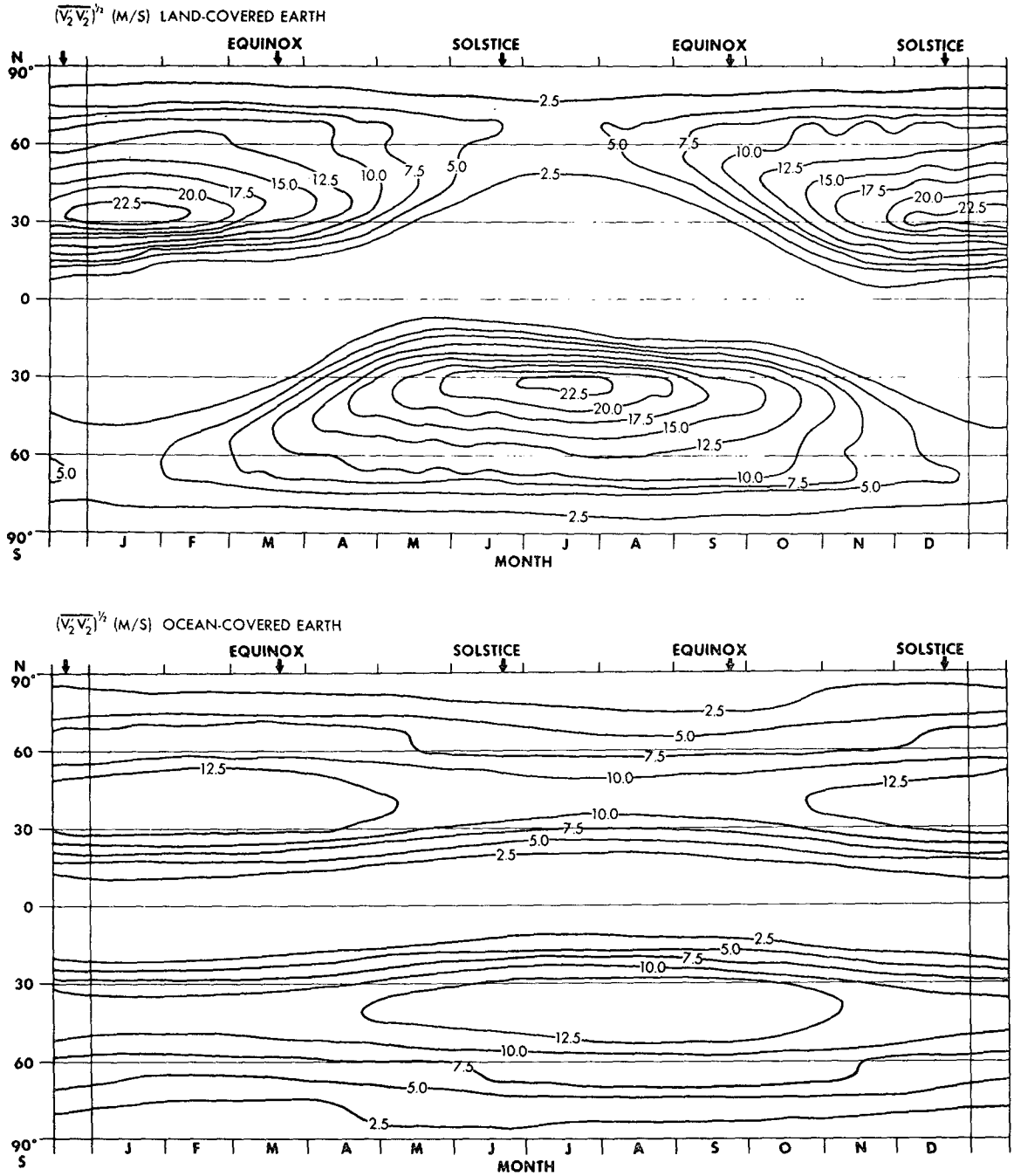

FIG. 14. Time variation of the latitudinal distribution of the standard deviation of the meridional component of wind, for LCE and OCE.

duced by the mean meridional circulation and by large scale eddy motion, are shown separately. From the figure it follows that the role of the meridional circulation in the hydrologic cycle is to provide a convergence of moisture into the tropical belt. At the June solstice, a large amount of moisture is transported into the summer hemisphere by the cross-equatorial flow in the lower part of a big Hadley cell. The moisture transfer, on the other hand, from the subtropics to higher latitudes, is produced solely by the large-scale eddies.

8. Variation of eddy statistics with time

a. Intensity of the eddies

In the present numerical model, the eddy kinetic energy is a predicted variable and the fluctuation in the

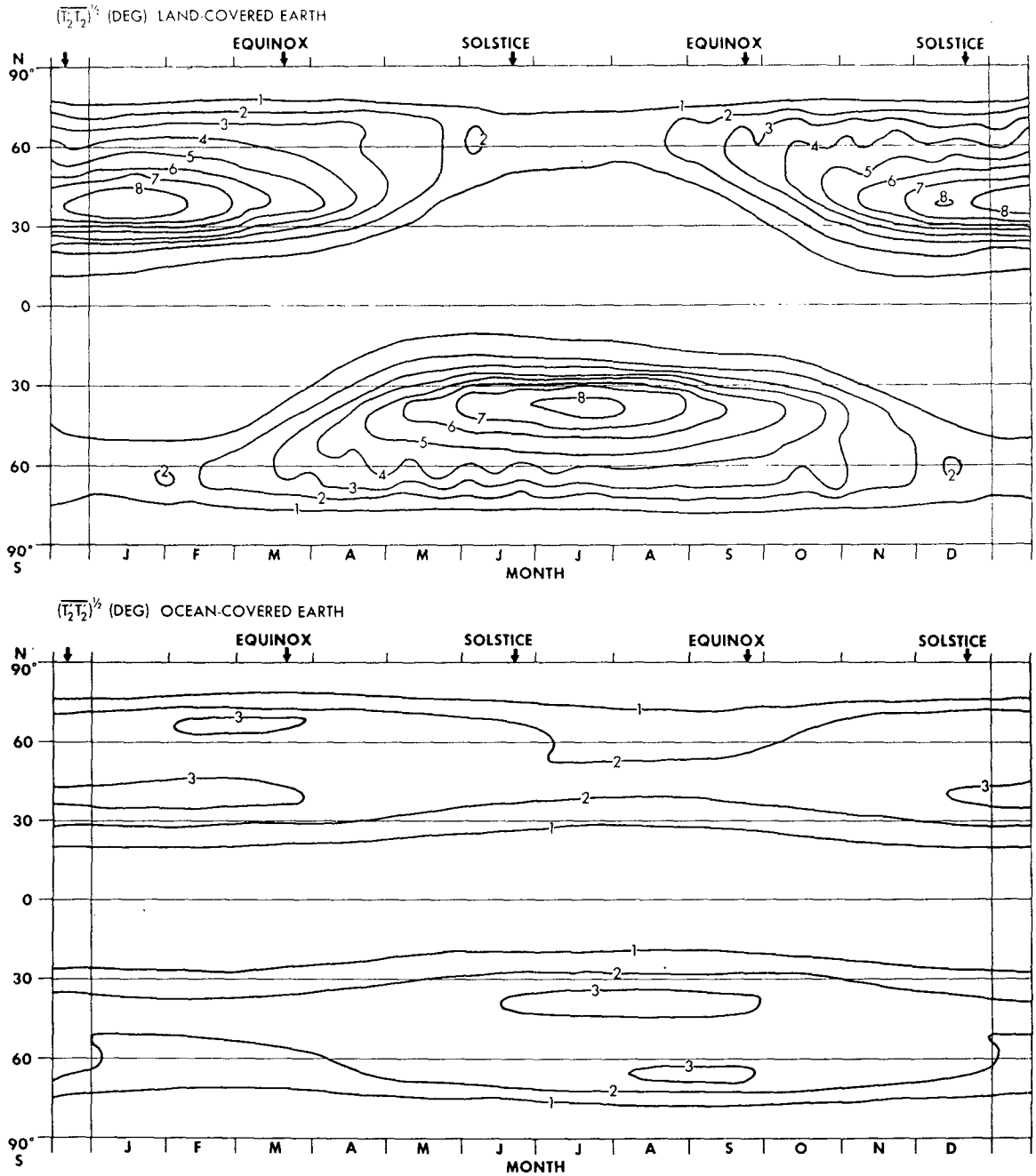

FIG. 15. Time variation of the latitudinal distribution of the standard deviation of temperature, for LCE and OCE.

TABLE 3. Eddy available potential energy (P_E; J cm^{-2}) and eddy kinetic energy (K_E; J cm^{-2}) for the Northern Hemisphere.

	Month												Annual
	Jan.	Feb.	Mar.	Apr.	May	June	July	Aug.	Sep.	Oct.	Nov.	Dec.	
P_E(Northern Hemisphere)													
Land-covered earth	145.2	123.5	72.2	39.1	11.6	3.8	3.1	3.9	12.4	40.5	88.0	127.2	55.9
Ocean-covered earth	26.3	27.4	26.1	22.1	16.5	12.9	10.9	10.2	11.4	14.7	19.6	23.8	18.5
K_E(Northern Hemisphere)													
Land-covered earth	287.4	249.7	165.7	96.7	32.6	10.3	9.0	13.6	34.3	98.9	204.6	266.4	122.4
Ocean-covered earth	117.1	120.9	115.6	99.1	76.8	61.5	53.2	51.5	56.5	69.0	88.6	106.8	84.7

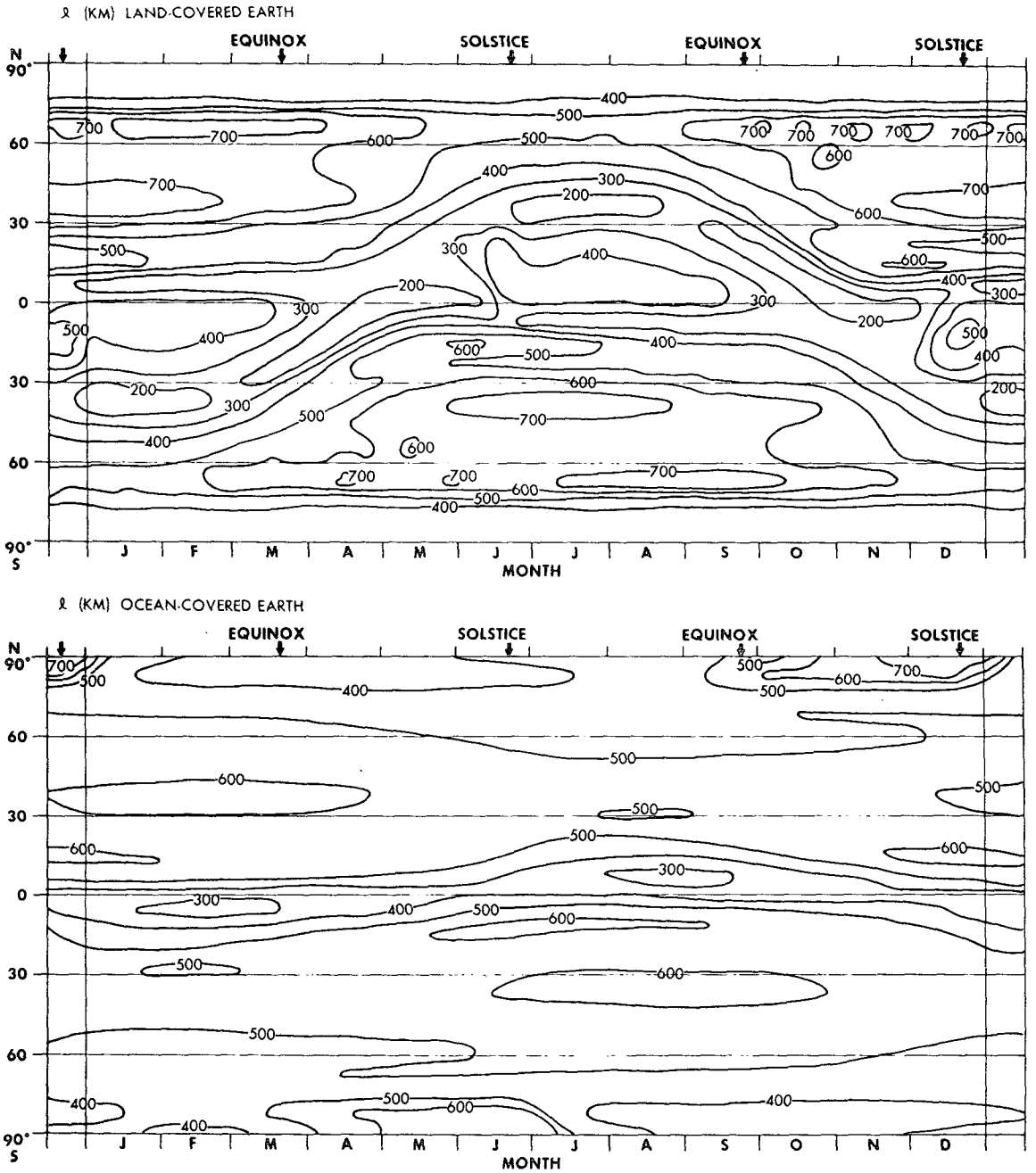

FIG. 16. Time variation of the latitudinal distribution of the characteristic scale of eddies, for LCE and OCE.

temperature field is obtained by a diagnostic formula. The variations of those quantities with latitude and time are shown in Figs. 14 and 15, respectively. The characteristic features of the two figures are quite similar to each other.

In the LCE, the seasonal change in the intensity of the eddies is large. Eddy motion becomes very weak during summer. In contrast to this, the amplitude of the eddies in the OCE does not vary much with time. Because the ocean moderates seasonal change, the eddy activity for the OCE is weaker than that for the LCE in winter and stronger in summer. This coincides with the variation of baroclinicity with time, as discussed in Section 4.

The monthly means of eddy available potential energy P_E and eddy kinetic energy K_E for the Northern Hemisphere for LCE and OCE are presented in Table 3. The annual range of variation (J cm^{-2}) is large for the LCE, from 3 to 145 for P_E and from 9 to 287 for K_E. The corresponding values for the OCE are from 10 to

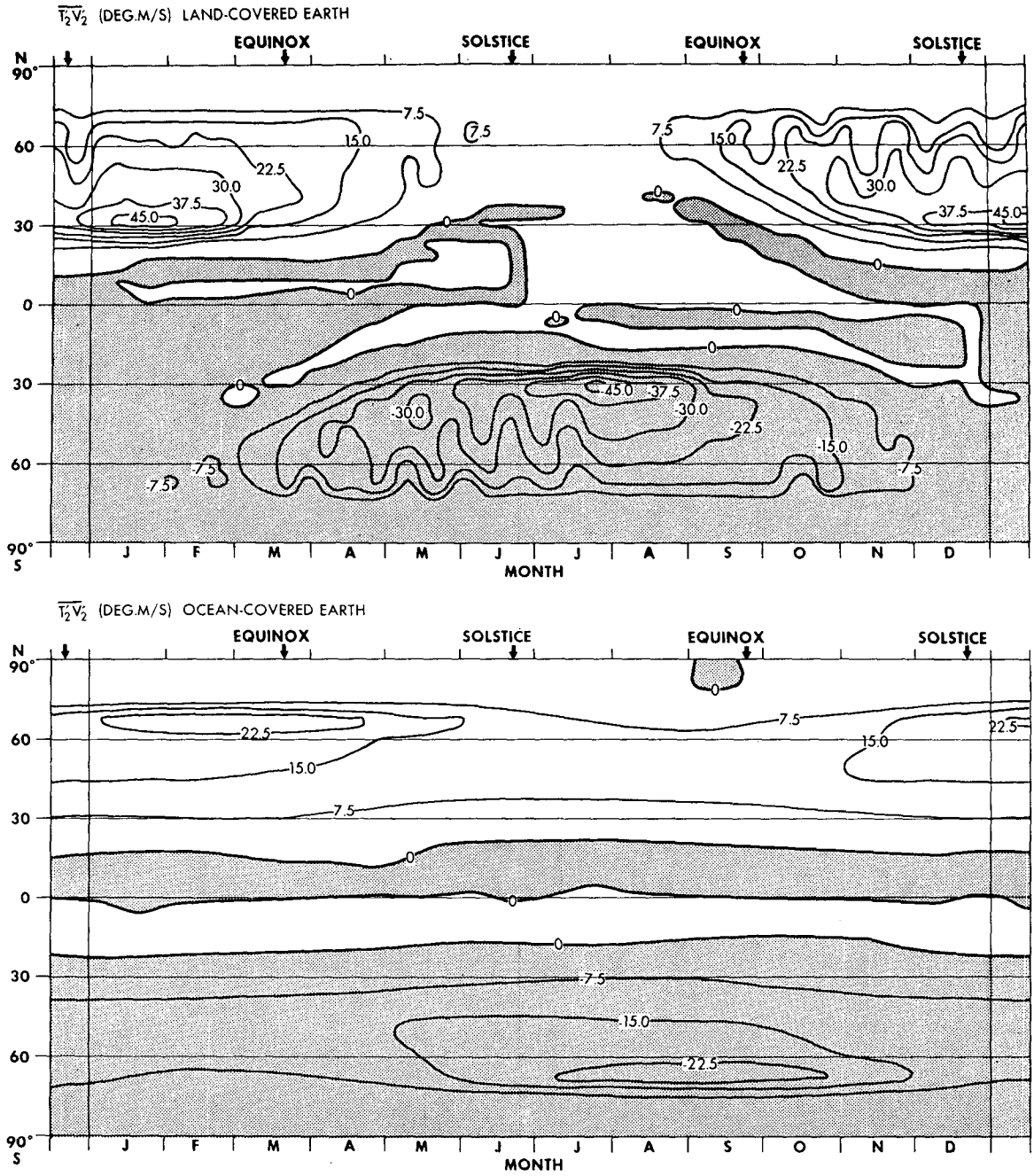

FIG. 17. Time variation of the latitudinal distribution of the meridional transport of heat due to the large-scale eddies, for LCE and OCE.

only 27 and from 52 to 121, respectively. Another difference between LCE and OCE is seen in the ratio of K_E to P_E. It is always about 5 for the OCE. The ratio is smaller for the LCE, namely 2–3. It may be interesting to note that K_E for the Northern Hemisphere of the LCE does not show a semi-annual cycle while K_Z does (Table 2). The time variation of K_E has a high correlation with that of westerly flow in middle latitudes. In the summertime, K_E decreases whereas K_Z increases because of the strong easterly flow at low latitudes. We also computed the global average of the eddy energies for each month. The global mean of P_E for the OCE is almost constant, from 18 to 19, while that of LCE varies within a range from 42 to 74. The range of variation of the global mean of K_E is also small for the OCE, i.e., 119–130, as compared with that for the LCE, i.e., 101–149.

From Tables 2 and 3, we can estimate the level of

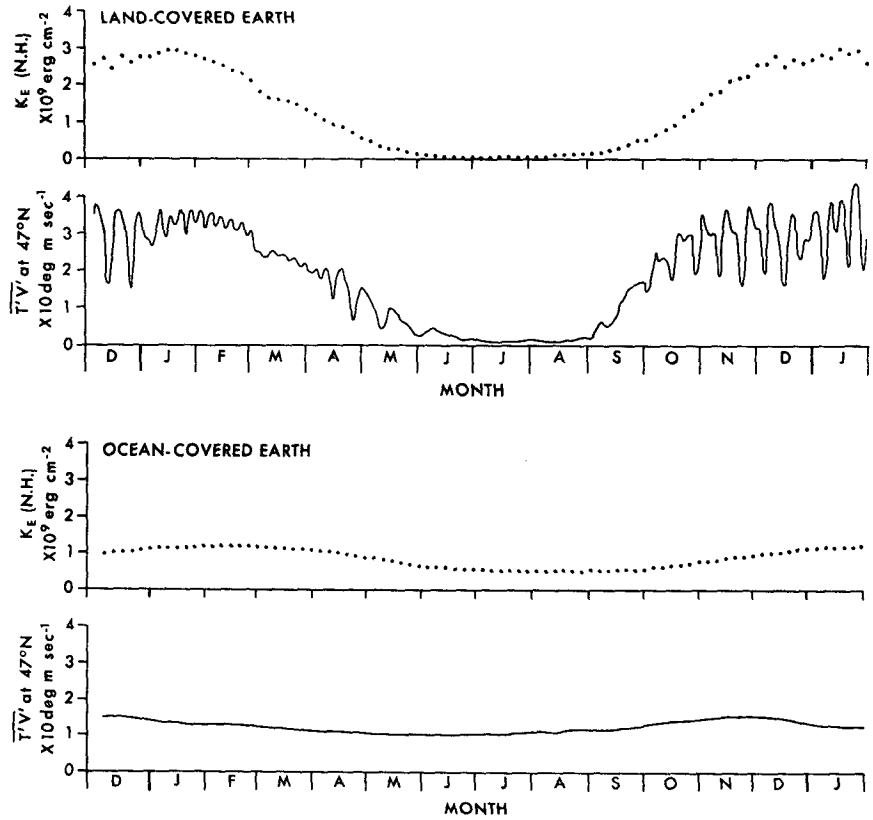

FIG. 18. Time variation of the mean eddy kinetic energy for the Northern Hemisphere and the eddy flux of heat at 47N, for LCE and OCE.

eddy kinetic energy in terms of its ratio to the kinetic energy of the zonal mean flow, K_Z. The ratio, $K_E \div K_Z$, for the Northern Hemisphere for the LCE is 1.0 or more during the period October through December and drops to 0.05 in summer. For the OCE, this ratio stays within a range 0.6–0.8.

b. Scale of eddies

In the present model, the characteristic scale of the eddies is computed from a diagnostic formula [Eq. (4.28) in K]. Its variation with time is shown in Fig. 16. The wavelength can be considered to be 2π times the scale. In middle latitudes, the scale becomes relatively small in summer for both LCE and OCE. But the seasonal change of scale is much larger for the LCE. The latitude of the minimum scale gradually moves from the middle latitudes of one hemisphere to the other as the season progresses in the LCE system. For the OCE, it is found at the tropics in all seasons.

c. Eddy transfer of heat

Fig. 17 shows the meridional transport of heat due to the large-scale eddies. A large amount of heat is transported poleward in the winter hemisphere of the LCE; the transport in summer is negligible.

In the case of OCE, a poleward transport of heat is seen at all latitudes except for a narrow tropical belt where a small countergradient heat flux occurs. The latitude of maximum poleward transport is further north of that of LCE. The flux in summer is about one-half that in winter.

It appears in Fig. 17 that the poleward eddy transfer of heat in the LCE fluctuates with time. In order to see it more precisely, the eddy flux of heat at 47N is shown in Fig. 18 together with the mean eddy kinetic energy for the Northern Hemisphere. The curve for the heat flux is based on daily values. For the LCE, the fluctuation of heat transfer has a period of 1–2 weeks. Its amplitudes changes apparently from one year to another. It is a common feature of both eddy kinetic energy and the heat transport that their increase in fall takes place in a shorter period as compared with the decrease after winter. In the OCE case, the heat transport as well as the eddy kinetic energy in summer is significantly larger than those in the LCE. Another interesting feature is that the short-period variation of the heat transport with time in the OCE is so small that it does not show up in the figure.

d. Eddy transport of momentum

In the present model, the meridional transport of momentum due to the large-scale eddies is estimated, in

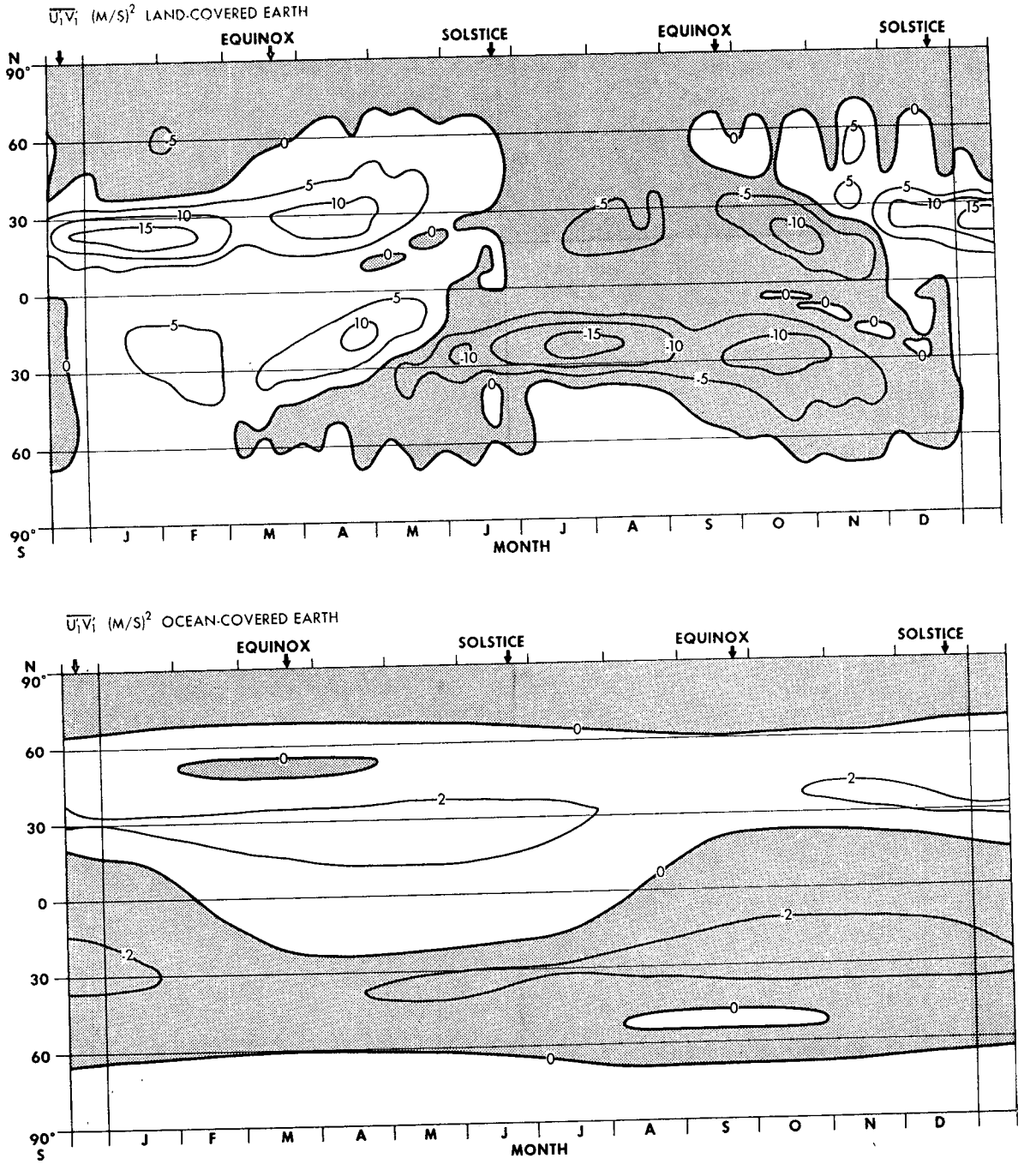

FIG. 19. Time variation of the latitudinal distribution of the meridional transport of momentum due to large-scale eddies, for LCE and OCE.

a passive manner, by making use of a diagnostic formula. It is determined mainly from the distribution of the surface pressure. The results are shown in Fig. 19.

For the LCE, the poleward transport of momentum occurs in winter and spring only. While for the OCE, a poleward transport occurs in middle latitudes irrespective of season, although its magnitude is small. At high latitudes, an equatorward flux is obtained both for the LCE and OCE.

9. Energetics

The budget analysis for the four conventional forms of energy is made by the usual method.

TABLE 4. Monthly statistics of the energy budget (10^{-3} J cm^{-2} day^{-1} mb^{-1}) for the Northern Hemisphere. The quantity $[K_Z,P_Z]$, however, is an estimate only for the global domain.

	Month												Annual
	Jan.	Feb.	Mar.	Apr.	May	June	July	Aug.	Sep.	Oct.	Nov.	Dec.	
Land-covered earth													
[heating, P_Z]	118.7	86.3	53.0	33.8	39.7	51.8	44.6	28.6	33.5	59.6	95.5	123.5	64.0
[P_Z, horizontal diffusion]	13.1	10.1	6.8	3.8	1.3	0.5	0.7	1.1	2.1	3.9	6.6	10.3	5.0
[P_Z,P_E]	111.0	96.6	58.6	32.8	10.6	3.7	2.5	4.1	15.8	42.3	74.0	92.8	45.4
[P_E, horizontal diffusion]	15.6	13.8	7.5	3.8	1.0	0.3	0.2	0.3	1.2	4.3	9.4	13.1	5.9
[P_E,K_E]	100.4	81.2	43.3	21.5	5.6	1.5	0.2	0.7	7.6	25.7	57.3	82.3	35.6
[K_E, horizontal diffusion]	58.7	50.6	28.4	14.8	4.6	1.3	1.3	2.2	5.4	16.5	35.3	49.1	22.4
[K_E, vertical diffusion]	2.8	2.1	1.1	0.5	0.1	0.0	0.0	0.1	0.1	0.5	1.6	2.6	0.9
[K_E, surface friction]	36.7	29.0	15.4	7.3	1.9	0.0	0.4	0.7	2.6	8.7	21.2	30.2	12.9
[K_E,K_Z]	2.5	1.5	0.8	1.6	0.3	0.0	−1.3	−2.0	−1.4	−2.8	−3.5	0.1	−0.3
[K_Z, horizontal diffusion]	10.1	7.5	3.4	1.5	0.4	0.2	0.5	0.7	0.9	1.0	1.8	5.4	2.8
[K_Z, vertical diffusion]	3.4	2.0	1.2	0.5	0.1	0.7	1.8	1.6	0.6	0.5	1.5	3.1	1.4
[K_Z, surface friction]	2.5	2.4	0.7	0.8	1.0	0.4	0.5	0.5	0.4	0.8	0.0	1.0	0.9
[K_Z,P_Z]	−8.8	−5.2	−2.3	−2.5	−5.4	−8.0	−8.3	−5.2	−2.4	−2.4	−5.5	−8.6	−5.4
Ocean-covered earth													
[hearing, P_Z]	33.5	33.5	31.2	27.5	25.5	26.0	27.5	28.0	27.1	26.3	27.4	30.9	28.7
[P_Z, horizontal diffusion]	4.7	5.4	5.4	4.3	3.0	2.0	1.5	1.4	1.5	1.9	2.6	3.6	3.1
[P_Z,P_E]	29.0	30.3	29.0	24.8	19.5	16.0	14.0	13.7	15.2	18.7	23.3	27.0	21.7
[P_E, horizontal diffusion]	2.9	3.1	3.0	2.5	1.8	1.4	1.1	1.1	1.2	1.6	2.1	2.6	2.0
[P_E, K_E]	21.8	23.2	22.1	18.3	13.4	10.4	8.9	8.8	9.8	12.4	16.2	19.6	15.4
[K_E, horizontal diffusion]	15.5	16.2	15.6	13.2	10.0	7.8	6.8	6.6	7.3	9.1	11.7	14.0	11.2
[K_E, vertical diffusion]	0.4	0.4	0.3	0.3	0.2	0.1	0.1	0.1	0.1	0.2	0.2	0.3	0.2
[K_E, surface friction]	6.1	6.6	6.3	5.1	3.6	2.6	2.1	2.0	2.2	2.9	4.0	5.2	4.1
[K_E,K_Z]	−0.3	−0.0	0.3	0.4	0.4	0.3	0.2	0.0	−0.1	−0.3	−0.4	−0.4	0.0
[K_Z, horizontal diffusion]	1.0	1.2	1.3	1.0	0.5	0.6	0.2	0.2	0.2	0.2	0.3	0.6	0.6
[K_Z, vertical diffusion]	1.4	1.5	1.4	1.0	0.6	0.3	0.2	0.2	0.3	0.4	0.7	1.1	0.8
[K_Z, surface friction]	0.1	0.2	0.3	0.3	0.3	0.3	0.2	0.2	0.1	0.1	0.1	0.1	0.2
[K_Z,P_Z]	−1.9	−1.9	−1.6	−1.3	−1.3	−1.5	−1.8	−1.9	−1.6	−1.3	−1.3	−1.5	−1.6

We can examine the energetics for a closed system by taking the global domain. However, we found that the variation of energy transformation with time was small in this case. In order to see the seasonal variation of energetics, we take a hemispheric domain. This means the domain is open and there exists interhemispheric exchange of energy.

In Table 4, the monthly statistics of the energy budget for the Northern Hemisphere are shown. The monthly mean values are the averages of daily statistics.

Generally speaking, for both LCE and OCE, the main direction of the energy transformation is [heating, P_Z], [P_Z, P_E], [P_E, K_E] and [K_E, dissipation] in this order. Dissipation of K_E is largely due to the horizontal diffusion of momentum. The contribution of surface friction to the dissipation of K_E is also significant but it is smaller than that of horizontal diffusion.

An exception to the above-mentioned main flow of energy is seen in the budget for May through August in the LCE. During this period, [P_Z, P_E] is fairly small as compared to the generation of P_Z due to heating. On the other hand, there is an occasional tendency in winter for the generation of P_Z to be insufficient for [P_Z, P_E]. Accordingly, it is likely that a leak of the total enthalpy from the summer into the winter hemisphere takes place in order to reduce P_Z in the summer hemisphere.

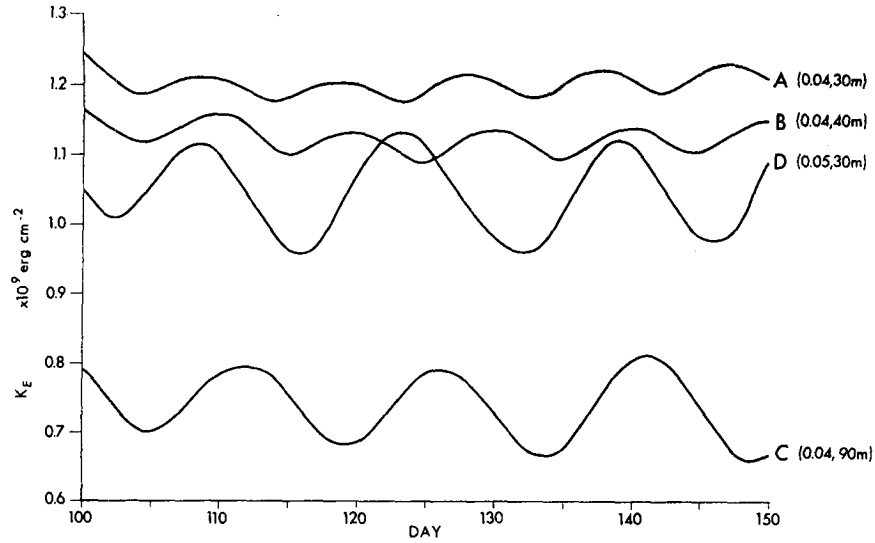

FIG. 20. Time variation of the mean eddy kinetic energy for the Northern Hemisphere for the 100–150 day period for LCE. Experiments are carried out for the annual mean insolation. Numbers in parentheses indicate the constants chosen for parameterizing the horizontal and vertical diffusion, respectively.

The energy conversion due to the baroclinic process, i.e., $[P_E, K_E]$, acts as the predominant source of K_E, always for the OCE and most of the time for the LCE. Only in July and August in the LCE, a contribution from the barotropic process, i.e., $-[K_E, K_Z]$, exceeds the transformation $[P_E, K_E]$, although both of them are small.

In the course of the analysis, it was found that the understanding of $[K_Z, P_Z]$ transformation for a single hemisphere was not a simple matter because of the cross-equatorial flow and the associated vertical motion in the hemispheric scale. This last quantity listed in Table 4 is an estimate for the entire global domain, not for the Northern Hemisphere. A negative value of $[K_Z, P_Z]$ indicates that, despite a small temperature gradient in the low latitudes, the energy transformation due to the Hadley circulation is larger than that due to the Ferrel cell which works in the opposite sense.

10. Experiments with different values of the eddy viscosity coefficients

In the experiment for LCE, many quantities displayed a fluctuation with a rather irregular period of around 10 days. In this section we will examine the dependence of the amplitude and period of K_E upon the coefficients chosen for parameterizing the sub-grid scale diffusion.

Four experiments were carried out with the LCE model. In these cases, the insolation was fixed at the annual mean value and the drag coefficient was set to be 0.0025. In experiments A, B and C, the constant which is used for calculating horizontal diffusion is the same, i.e., 0.04, but the mixing length at the middle level is different, i.e., 30, 40 and 90 m, respectively. Experiment D is different from A in that the coefficient in the formula for horizontal diffusion is 0.05 instead of 0.04.

Variation of the hemispheric mean of K_E with time for the period of 50 days in each experiment is shown in Fig. 20. It is seen from the figure that the level of K_E falls as the atmosphere becomes more viscid. The amplitude of the fluctuation becomes larger when the coefficient for either vertical or horizontal diffusion is increased. At the same time, the period of oscillation becomes longer. These results suggest the necessity of careful specification of the parameters for diffusion in a numerical model of the atmosphere.

11. Aftereffect of a sudden shock to the OCE model

It has been shown that short-period oscillations of the meteorological quantities in the OCE are very weak. Thus, a sudden shock must be applied to this model to produce a sizeable fluctuation. We will examine how long it takes before the aftereffect of a shock becomes unnoticeable in the model. This may give a rough measure of the length of memory of the model atmosphere.

The solid curve in Fig. 21 represents the eddy transport of heat at 47N in the third year of the integration. The result for the fourth year is almost an exact repetition of that for the third year until a shock was given. The drag coefficient was increased on 19 February from 0.0011 to 0.0043 which was the value used for LCE. This increased value was used in the following 10 days. Then, on 1 March, it was reduced to the previous value, i.e., 0.0011. In other words, the brake being applied to the moving atmosphere at the

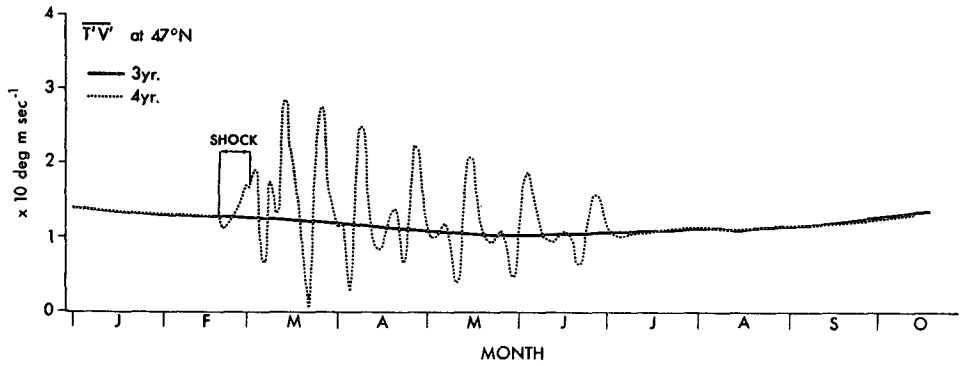

FIG. 21. Time variation of the eddy transport of heat at 47N for the third and fourth years for OCE. The period when a shock was given to the model in the fourth year is indicated.

surface of the earth was intensified during the 10-day period.

As shown by the dotted line in Fig. 21, the eddy transfer of heat started to oscillate after the shock. As time goes on, the amplitude of oscillation gradually decreases and its period becomes longer. Finally, about 5 months after the shock, it settles down to a state similar to that of the third year. Accordingly, we infer that, as far as the present model of OCE is concerned, the time scale of atmospheric inertia is about 5 months.

12. Summary

Using a statistical-dynamical model of the atmosphere, numerical experiments were carried out to examine the seasonal variation of the global atmospheric circulation. The experiments were made both for a land-covered and an ocean-covered earth. The differences between the two models are: drag coefficient (0.0043 and 0.0011, respectively), thermal condition at the surface (zero heat capacity and specified sea-surface temperature, respectively), and the hydrologic cycle (considered at OCE only).

The results were analyzed for many quantities in a form of the variation of the latitudinal distribution with time. Baroclinicity at the middle latitudes is seen in summer for the OCE only. A big difference, qualitative rather than quantitative, is found in the field of zonal mean flow in low latitudes. At the upper level, a strong easterly flow evolved in the LCE, but not in the OCE. A main feature of the mean meridional circulation for both LCE and OCE is the big Hadley cell in summer and in winter. The Ferrel cell is observed the whole year in the OCE. The Ferrel circulation in the LCE is strong and fluctuates in winter, and disappears in summer. In the OCE, the moisture is transported equatorward from the subtropics by the mean meridional circulation and poleward by the large-scale eddies. The seasonal variation of certain eddy statistics such as the eddy kinetic energy and the eddy transport of heat is moderated in the OCE. As a result, the eddy activity in winter in the OCE is weaker in every respect than that in the LCE. It is noticeable in the OCE in summer when it is not observable in the LCE.

The above results clearly show the importance of the earth's surface condition on the atmospheric circulation, i.e., how large an influence the ocean exerts on the seasonal variation of the global circulation of the atmosphere. A further experiment also suggests that the specification of parameters for the internal diffusion is important in modeling the atmosphere.

An additional experiment gives an estimate of the length of memory of the atmosphere of the OCE when a sudden shock is given. It is approximately 5 months.

Finally, it should be remarked that the monsoon-type phenomena which are associated with land-sea distribution cannot be treated by the present model, but only by an orthodox numerical model (e.g., Wetherald and Manabe, 1972).

Acknowledgments. The author is deeply indebted to J. Smagorinsky and S. Manabe for the encouragement he received throughout this study. He thanks A. Oort, R. T. Wetherald and G. P. Williams for giving him valuable comments on the original manuscript. Thanks are also due to E. J. D'Amico for typing the manuscript and to W. H. Moore and P. G. Tunison for preparing the figures.

APPENDIX

Remarks on the Empirical Formulas and Numerical Schemes

The empirical formulas used in Section 2 were derived by a trial-and-error method. It is important, however, that they give reasonable estimates for any season and latitude. For example, when the observed values of temperature and static stability at the 500-mb level at a certain time and latitude are substituted for $\bar{T}_2$ and Γ_2 in (2.2), the computed value of $\bar{T}_{1000}$ should be as near as possible to the observed temperature at the 1000-mb

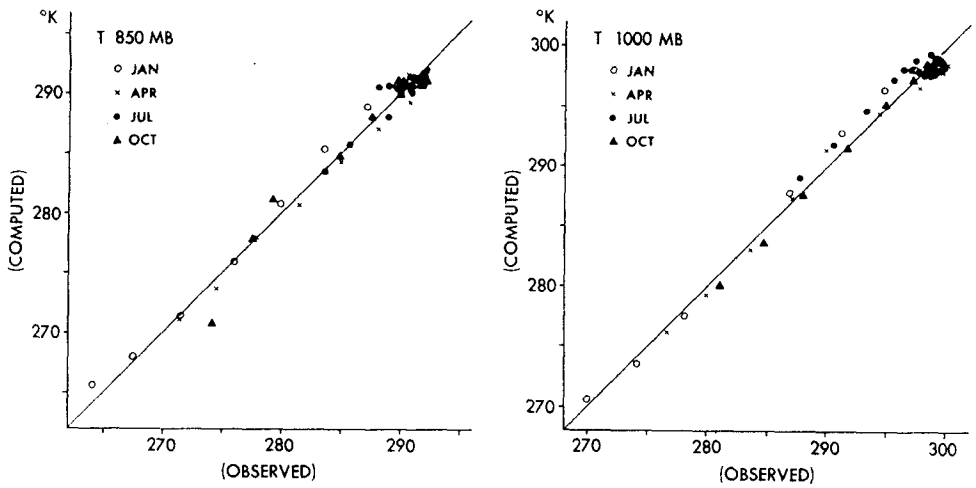

FIG. A1. Scatter diagram of the observed temperature at the 850 mb surface (left) and at 1000 mb (right) and the temperature computed from the empirical formula. The perfect-fit line is indicated by a straight line.

level at the corresponding time and latitude. Differences between the computed and the observed values were minimized by determining the numerical constants involved in the formulas by the least-squares method. This method was applied to the data for four seasons and for latitudes from 10S through 60N. The comparison between the computed and observed values are presented in Figs. A1–A3. It is seen that the empirical formulas can give a good estimate if the input data are correct.

When we use the empirical formulas, the resulting values have to be checked by a certain criterion and adjusted if necessary. In using (2.5) and (2.6), if the multiplying factor to the saturation mixing ratio exceeded 1.0, it was simply set to be 1.0. The evaporation rate was adjusted to 0.00033 gm cm^{-2} day^{-1}, if it tended to be less than that. Furthermore, when P computed by (2.9) took on negative values, E was increased to give a zero value for P.

The numerical schemes we used for the integration are the same as those described in the previous paper (1970). An estimate of the transport of moisture by the

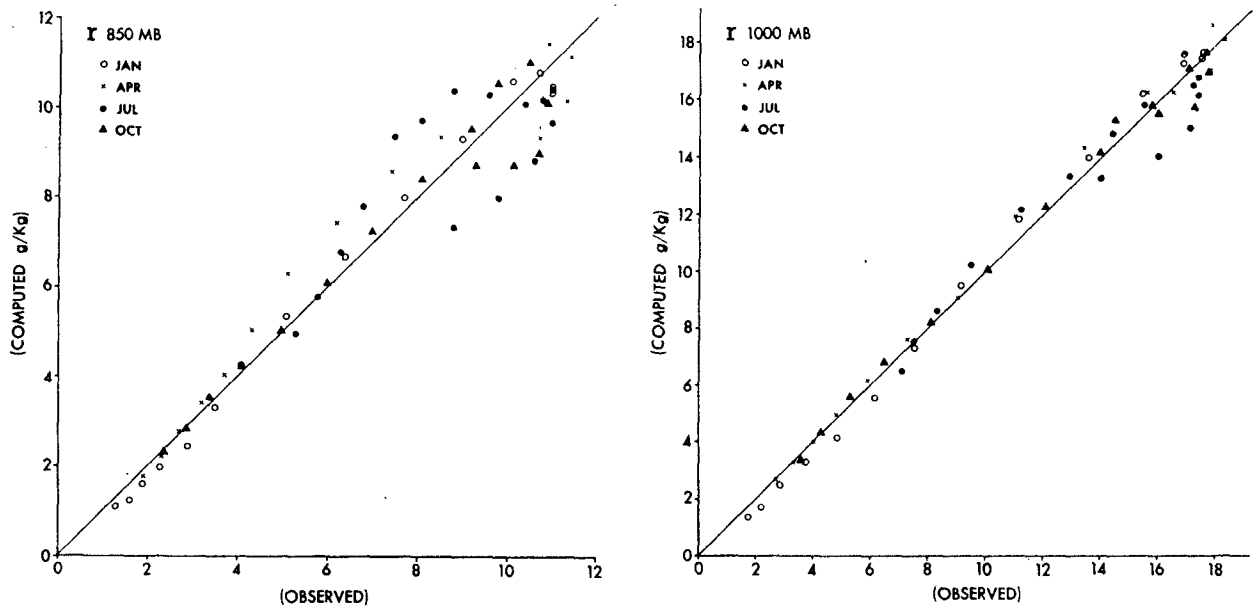

FIG. A2. Same as Fig. A1 except for the mixing ratio at the 850 mb surface (left) and at 1000 mb (right).

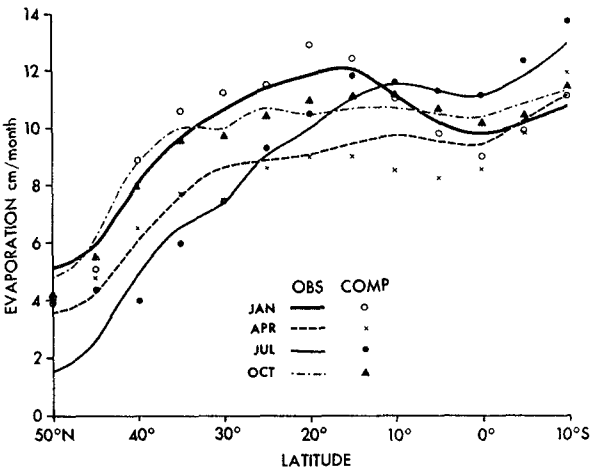

FIG. A3. Latitudinal distribution of the zonal mean evaporation obtained from climatological statistics (OBS) and computed by an empirical formula (COMP).

mean meridional circulation, i.e., the first factor on the right-hand side of (2.8), was made with the same scheme as used for the term for the transport of eddy kinetic energy (see Appendix 3 in K).

REFERENCES

Bryan, K., 1959: A numerical investigation of certain features of the general circulation. *Tellus*, **11**, 163–174.

Kraus, E. B., and E. N. Lorenz, 1966: Numerical experiments with large-scale forcing. *J. Atmos. Sci.*, **23**, 3–12.

Kurihara, Y., 1970: A statistical-dynamical model of the general circulation of the atmosphere. *J. Atmos. Sci.*, **27**, 847–870.

——, 1971: Seasonal variation of temperature in an atmosphere at rest. *J. Meteor. Soc. Japan*, **49**, 537–544.

Oort, A. H., and E. M. Rasmusson, 1971: Atmospheric circulation statistics. NOAA Prof. Paper No. 5, U. S. Dept. of Commerce.

Saltzman, B., and A. D. Vernekar, 1971: An equilibrium solution for the axially-symmetric component of the earth's macroclimate. *J. Geophys. Res.*, **76**, 1498–1524.

Wetherald, R. T., and S. Manabe, 1972: Response of the joint ocean-atmosphere model to the seasonal variation of the solar radiation. *Mon. Wea. Rev.*, **100**, 42–59.

Wiin-Nielsen, A., 1970: A theoretical study of the annual variation of atmospheric energy. *Tellus*, **22**, 1–16.